Interdecadal Variations in Arctic Sea ice

Ignatius G. Rigor

A dissertation
submitted in partial fulfillment of the
requirements for the degree of

Doctor of Philosophy

University of Washington

2005

Program Authorized to Offer Degree:

Department of Atmospheric Sciences

University of Washington
Graduate School

This is to certify that I have examined this copy of a doctoral dissertation by

Ignatius G. Rigor

and have found that it is complete and satisfactory in all respects,
and that any and all revisions by the final
examining committee have been made.

Chair of Supervisory Committee:

John M. Wallace

Reading Committee:

John M. Wallace

David Battisti

Jamie Morison

David A. Rothrock

Date:_____

In presenting this dissertation in partial fulfillment of the requirements for the doctoral degree at the University of Washington, I agree that the Library shall make its copies freely available for inspection. I further agree that extensive copying of the dissertation is allowable only for scholarly purposes, consistent with "fair use" as prescribed in the U.S. Copyright Law. Requests for copying or reproduction of this dissertation may be referred to Proquest Information and Learning, 300 North Zeeb Road, Ann Arbor, MI 48106-1346, or to the author.

Signature_____

Date_____

University of Washington

Abstract

Variations in Arctic Sea ice

By Ignatius G. Rigor

Chairperson of the Supervisory Committee: Professor John M. Wallace
Department of Atmospheric Science

Sea ice has a profound effect on wildlife and people who live and hunt in the Arctic. The sea ice also plays a crucial role in global climate system, because of its role in maintaining the global heat balance and its affect on the global ocean thermohaline circulation. Arctic sea ice extent and thickness have decreased dramatically in the 1990's. The decline of the Arctic sea ice pack may be attributed to the observed increase in surface temperature, but it may also be caused by a simple shift in the winds over the Arctic Ocean such that the older, thicker sea ice is exported from the Arctic Ocean to the warmer waters of the North Atlantic.

In this dissertation, a hypothesis is advanced that the decline of arctic sea ice pack was dynamically induced by changes in the surface winds over the Arctic Ocean. Using a simple model, it is shown that the areal coverage of thick, multi-year ice decreased precipitously during 1989-1990 when the Arctic Oscillation was in an extreme "high index" state, and has remained low since that time. Under these conditions younger sea ice recirculates back to the Alaskan coast more quickly, decreasing the time that new ice has to ridge and thicken before returning for another melt season. During the 2002 and 2003 summers this anomalously young, thin sea ice

was advected into Alaskan coastal waters where extensive melting was observed, even though temperatures were locally colder than normal. We show that changes in sea ice driven by variations in wind related to the Arctic Oscillation appear to be the primary factor forcing the observed decreases in sea ice thickness, and thus the increases in surface air temperature and the decreases in sea ice extent that have been observed since 1989. Dynamically induced variations in the age of sea ice explain more than half of the variance in summer sea ice extent.

TABLE OF CONTENTS

LIST OF FIGURES

ACKNOWLEDGEMENTS

I would like to thank my dissertation advisor, Professor John M. Wallace, for his invaluable support and guidance, Professors David S. Battisti, Dennis Hartmann, Jamie Morison, and David A. Rothrock for serving on my supervisory committee, LuAnne Thompson for serving as my graduate school representative, Cecilia Bitz, Roger L. Colony, Dennis Hartmann, Sue Huney, Seymour Laxon, Ron Lindsay, Seelye Martin, Todd Mitchell, Richard E. Moritz, Mark Ortmeyer, Axel Schweiger, Mark C. Serreze, Harry Stern, Mike Timlin, Norbert Untersteiner, John Walsh, Steve G. Warren, Rebecca Woodgate, Jinlun Zhang, and others too numerous to mention here for their advice, encouragement and support. I would also like to thank Jeff Simmen, Robert C. Spindel, the late John C. Harlett, and Bob Odom for awarding me the Applied Physics Laboratory Graduate Fellowship, which has supported me in this endeavor.

I would also like to thank my friends, especially Bob Bratager for his guidance and support throughout my career, Ioana Dima and Robb Contreras for helping me remember how to add, Paul for dragging me out to play, and mom and dad for making me who I am. And I would like to thank my wife Brenda for her love and support, and my son Seth for bringing new wonder and meaning to my life. ...wa doo!

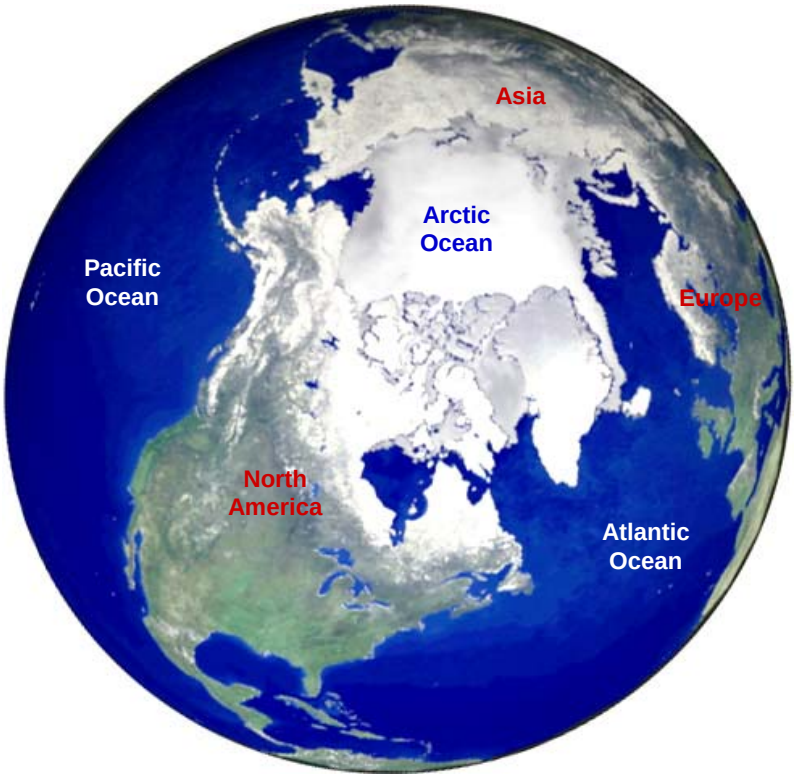

Figure 1. Satellite (RadarSat) image of the Earth showing the sea ice covered Arctic Ocean. Source: http://photojournal.jpl.nasa.gov/.

1. Introduction

One of the most striking features of the Earth is the sea ice covered Arctic Ocean (Fig. 1). Sea ice has a significant impact on wildlife and people. Many species and cultures depend on the sea ice for habitat and subsistence. For example, Inupiat hunt for bowhead whales (Fig. 2), and polar bears hunt and raise their young on the sea ice (Figs. 3 and 4). The lack of sea ice in an area along the coast may expose the coastline to ocean waves, which may threaten low lying coastal towns and accelerate the rate of erosion (Lynch et al. 2003). And from an economic viewpoint, the extent of

Figure 2. An Inupiat hunting for bowhead whales off Point Barrow, Alaska. *"As the favored East wind gives way to a breeze from the west, Kunuk studies ice advancing towards camp. After concluding that the advancing ice poses a threat to the safety of his crew, he gives the order to abandon camp. When conditions grow suddenly hazardous, a crew can pack up and evacuate a camp in as little as 15 minutes."* - Bill Hess, Gift of the Whale: The Inupiat Bowhead Hunt, A Sacred Tradition. Photo by Bill Hess, source: http://dirckhalstead.org/.

Figure 3. A polar bear hunting along a large ridge of sea ice. Source: http://atlas.ec.gc.ca/.

Figure 4. Polar bears emerging from their den in an area of heavily ridged sea ice. Photo courtesy of Steven Amstrup, U.S. Geological Survey.

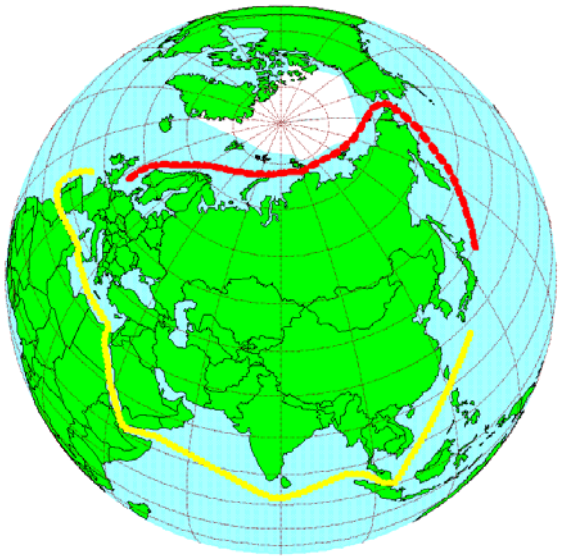

Figure 5. Shipping routes from Europe to Asia through the Northern Sea Route (red), and through the Suez Canal (yellow). Source: http://www.fni.no/insrop/.

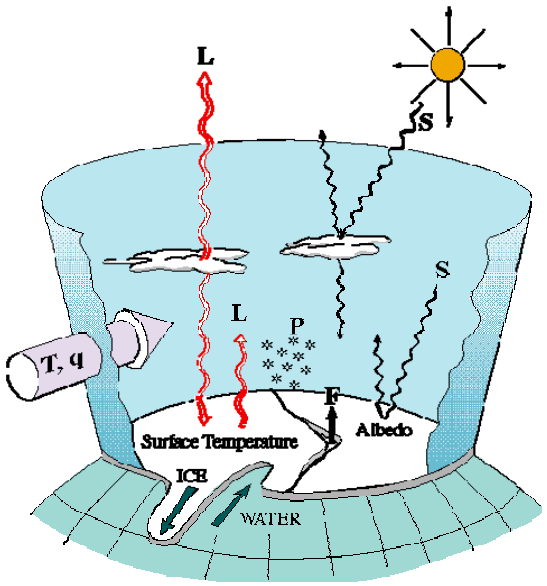

Figure 6. Arctic connections to global climate. Excess heat (temperature, T, and humidity, q) absorbed at lower latitudes is transported poleward by the atmosphere and ocean where it is radiated back out to space (long wave radiation, L). Sea ice over the Arctic Ocean insulates the atmosphere from the ocean thus reducing the amount of heat lost to space, but also has a higher albedo than the ocean, which reduces the amount of heat absorbed by the ice covered ocean (shortwave radiation, S). Most of heat from the ocean escapes into the atmosphere through the cracks in the sea ice (heat flux, F). Figure courtesy of Norbert Untersteiner.

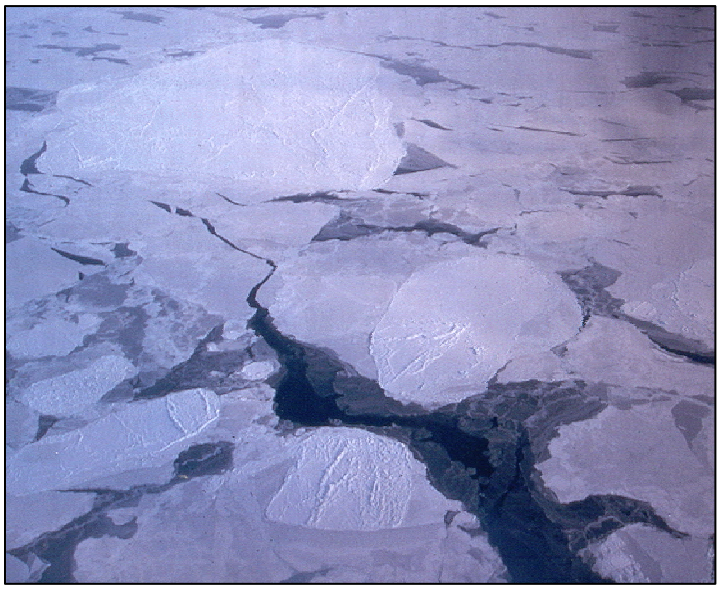

Figure 7. Sea ice of different ages. The larger, white sea ice floes with snow and ridges are older, multi-year sea ice; the darker, flatter patches of sea ice are younger, first year sea ice; and a few areas of open water can also be seen (darkest areas).

Arctic sea ice affects navigation from the Atlantic to the Pacific through the Arctic along the Northern Sea Route and Northwest Passage, which are as much as 60% shorter than the conventional routes from Europe to the west coast of the U.S. or Japan (Fig. 5).[*]

The Arctic also plays an important role in the global climate system, primarily through its role in the global heat balance and by its effect on the global thermohaline circulation (Aagaard and Carmack, 1994). Figure 6 shows some of the connections between the Arctic and the global climate system. Excess latent and sensible heat from the sun absorbed at lower latitudes is transported poleward by the atmosphere and ocean where it is radiated back out to space (Fig. 6). Sea ice over the Arctic Ocean insulates the atmosphere from the ocean thus reducing the amount of heat lost to space. Sea ice also has a higher albedo (reflectivity) than the darker ocean (e.g. Figs. 1 and 7), thus reducing the amount of sunlight absorbed by the sea ice covered ocean. A decrease in sea ice would increase the exposed area of the darker ocean, increasing the amount of sun light absorbed, thus warming the ocean, melting more sea ice, and amplifying the initial perturbations (ice-albedo positive feedback). However, the moisture fluxes into the atmosphere (Fig. 6) are also higher over open water than over sea ice, which may increase the areal coverage of fog and low clouds, increasing the albedo near the surface, and damping the initial perturbations (cloud-radiation negative feedback). These opposing feedbacks underscore the complexity of the Arctic and global climate systems.

[*] Approximately 12000 km. compared to 34000 km. around Cape Horn.

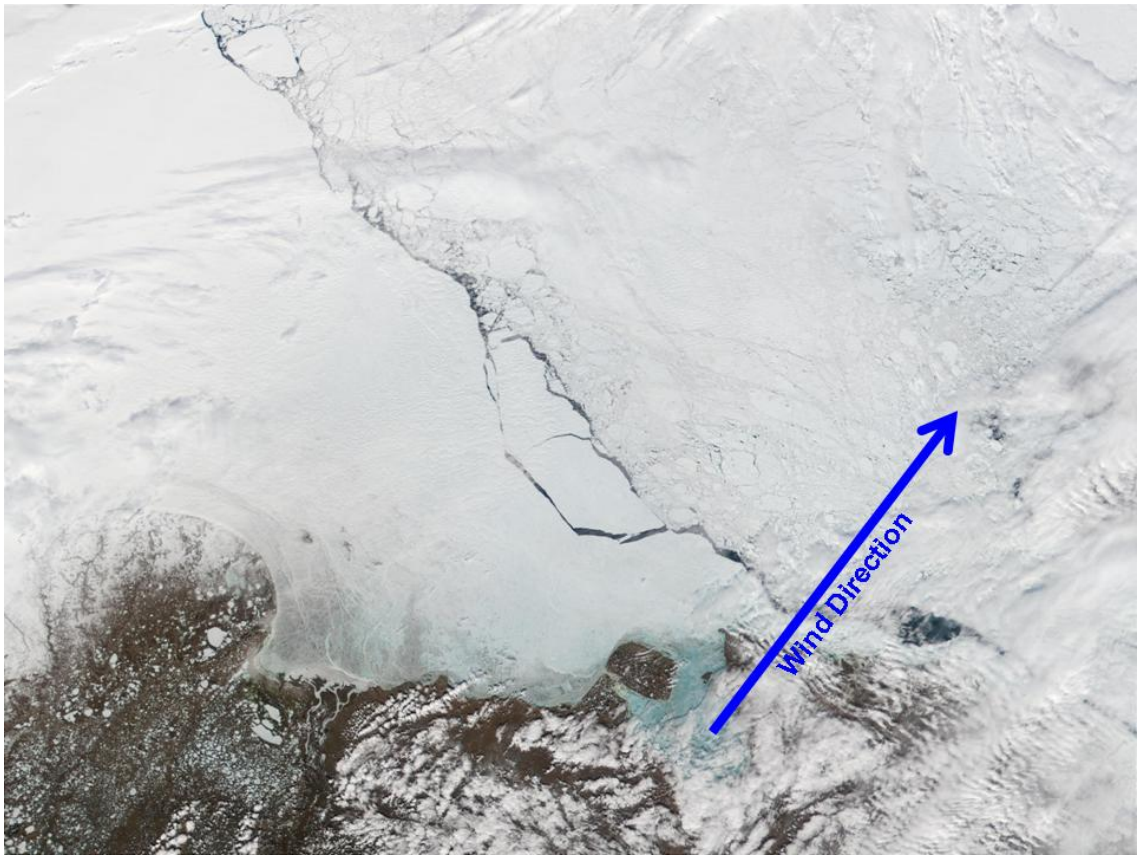

Figure 8. MODIS satellite image of the East Siberian Sea along the Russian coast of the Arctic Ocean. A large crack is forming as the winds blow the drifting sea ice away from the landfast ice edge. The thinnest ice appears bright blue because some light is able to penetrate and reflect off the water beneath. The scale of this picture is on the order of a thousand of kilometers. Source: Jacques Descloitres, MODIS Land Rapid Response Team at NASA/GSFC, http://visibleearth.nasa.gov.

The state of the Arctic sea ice pack is determined by the effects of the atmosphere and ocean upon the sea ice on various time scales. As the sea ice drifts over the Arctic Ocean, its motion is driven primarily by the surface winds (Fig. 8), which account for 70% of the day-to-day variance (Thorndike and Colony, 1982). On time scales of days to weeks, wind stresses from storms (e.g. Shy and Walsh, 1996) produce ridges, which thicken sea ice (Figs. 3, 4 and 7), and areas of open water (Figs. 7 and 8),

which freeze up quickly during winter, thereby increasing the overall volume of sea ice within a specified area. During spring and summer the presence of open water allows more solar energy to be absorbed and stored in the ocean mixed layer, thereby prolonging the melt season, and further increasing the annually integrated absorption of solar radiation. Ridging tends to occur preferentially during storms when the wind stress is strong enough to produce large deformations in the sea ice (Fig. 8). The number of storms that any given parcel of ice has experienced is cumulative, and hence the amount of ridged ice tends to increase with the age of the ice. The thicker, ridged ice provides stronger insulation for the atmosphere, but a significant amount of heat is still lost to the atmosphere through the cracks in which new sea ice may form (Figs. 6, 7. and 8).

As sea ice grows salt is released from the ice to the ocean. The fresher sea ice is then transported towards Fram Strait and the convective regions in the Greenland and Labrador seas (North Atlantic, Figs. 1 and 6). The melting ice provides a source of fresh water, which is less dense than sea water and may hinder the formation of deep water, thereby slowing the global thermohaline circulation (e.g. Aagaard and Carmack, 1994; Kwok and Rothrock, 1999; Belkin, 2004).

a. Arctic Climate Change

Climate change in the Arctic may be a harbinger of global climate change. Simulations by Manabe et al. (1991) with a global climate model predict that the transient response of climate to an increase in the concentration of atmospheric CO_2 at a

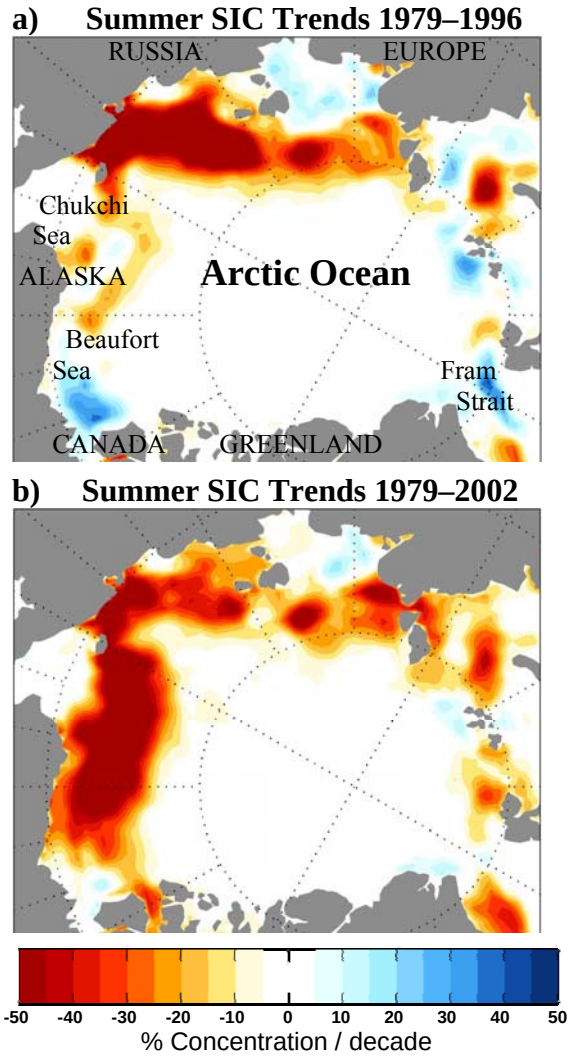

Figure 9. Trends in Summer sea ice concentration from microwave satellite data from 1979–1996 as shown by Parkinson et al. 1999 (a), and the updated trends for 1979–2002 (b).

rate of 1% per year would cause the Arctic to warm by more than 5°C, compared to a warming of 2°C for subpolar regions, by the time CO_2 concentrations doubled. This enhanced warming of the Arctic is attributed to the ice-albedo feedback.

The Inuit have observed that sea ice on the Arctic Ocean has changed dramatically during the last decade. "Solid ice has disappeared and there are no longer huge icebergs during autumn and winter. The ice now comes later and goes out earlier and it is getting thinner" (Wongittilin, 2000). These changes have a profound impact on the ability of Inuits to hunt and sustain their culture. Quantitatively, this "traditional knowledge" is supported by the observed decreases in sea ice thickness (Rothrock, et al. 1999) and sea ice extent (Parkinson, et al. 1999; Fig. 9a), and increases in winter, spring and autumn surface air temperature (Rigor et al. 2000; Fig. 10 left column). These changes have been attributed to global warming, which may have thinned and decreased the area of sea ice, but perhaps the tendency toward a thinner and less expansive area of sea ice has allowed more heat to escape from the ocean and warm the overlying atmosphere.

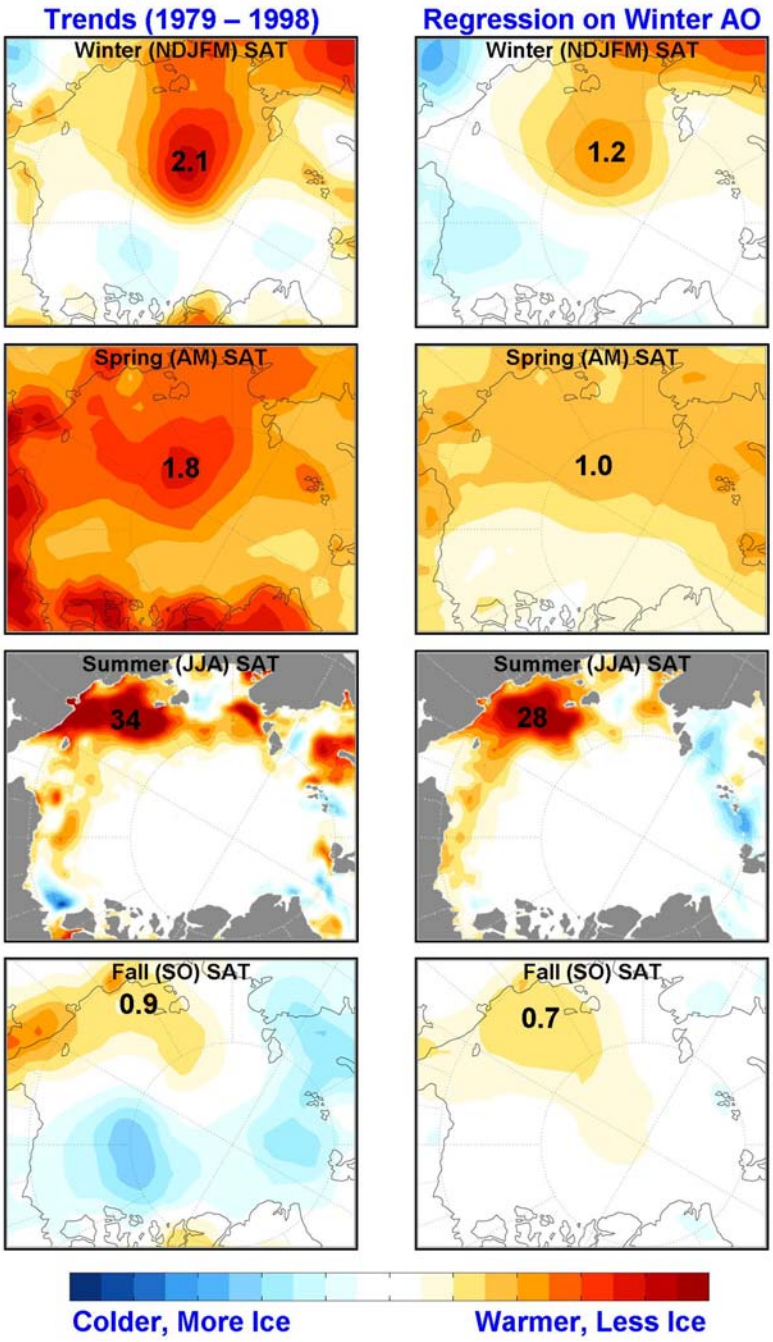

Figure 10. Seasonal trends in surface air temperature and sea ice extent 1979–1998 (left column), and the regression of these fields on the winter Arctic Oscillation index (right column). The winter regression map is on the concurrent winter AO index, while the regressions for the subsequent seasons are on the prior winter AO index. Units: trends are in °C/decade and %/decade; regressions are °C/decade and %/decade per standard deviation of the AO index.

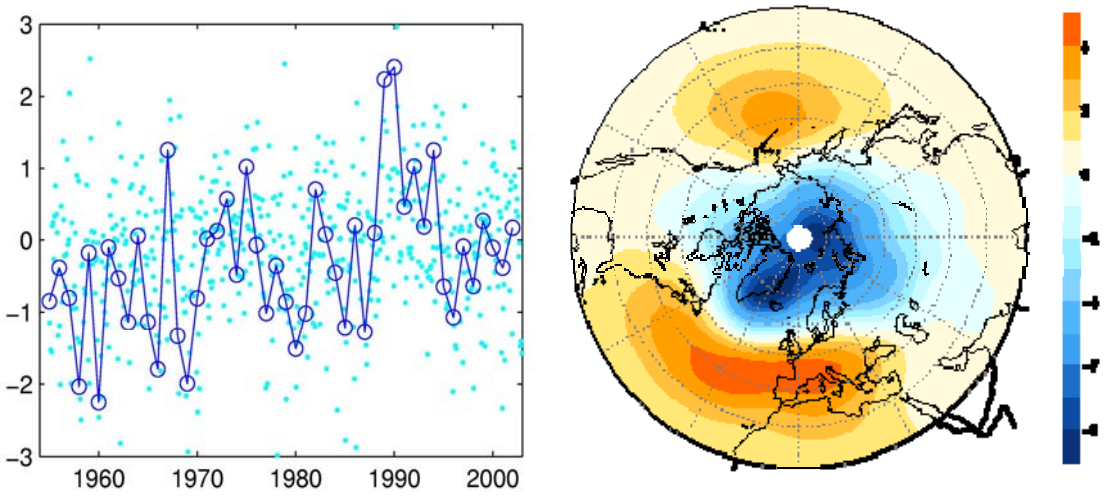

Figure 11. Arctic Oscillation (AO) index from 1955–2002 (left), and the regression map of sea level pressure on the winter (JFM) AO index (right). The monthly AO index is shown as cyan dots, and the year-to-year mean of these values is shown as open circles.

b. The Arctic Oscillation and Dynamically Induced Climate Change

Many of the observed changes in arctic climate have been linked to variations in large-scale atmospheric circulation related to the Arctic Oscillation (AO, Thompson and Wallace, 1998), whose index is defined as the leading principal component of Northern Hemisphere sea level pressure (Fig. 11). The AO can be characterized as an exchange of atmospheric mass between the Arctic Ocean and the surrounding zonal ring centered ~45°N. The AO exhibits a considerable amount of variability from month-to-month (Fig. 11), and there has been a trend towards higher AO conditions consistent with a tendency towards more cyclonic winds over the Arctic Ocean (Fig. 12). The decrease in sea level pressure over the Arctic Ocean (Walsh et al. 1996) coincides with

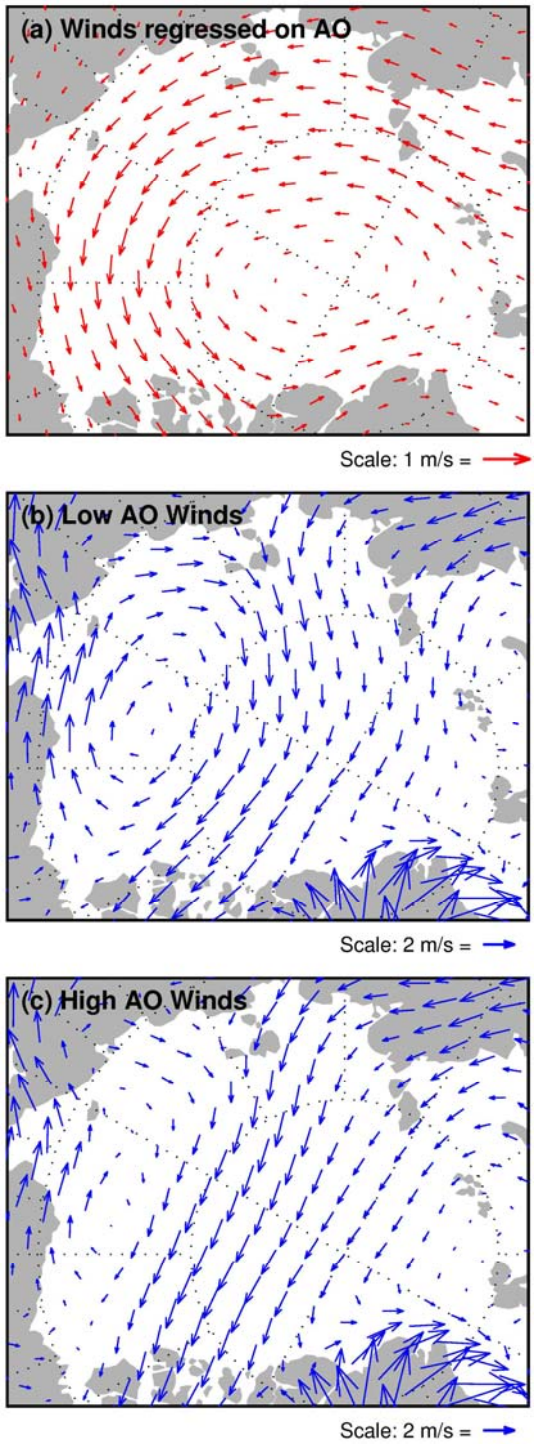

Figure 12. Regression map of 925 hPa winds on the winter AO index for all months (a), and composites of low and high AO winds (b and c).

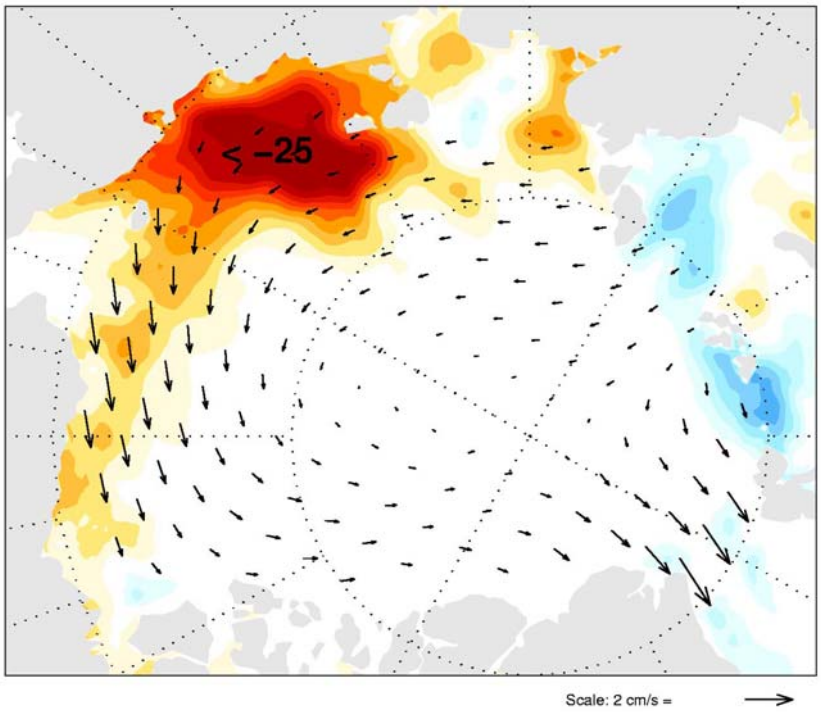

Figure 13. Regression maps of summer sea ice concentration and prior winter sea ice motion from 1979–1998 on the prior winter Arctic Oscillation index.

the step in the AO index in 1989. The AO explains more than 54% of the variance in SLP during winter and over 36% during summer over the Arctic Ocean, and thus many of the changes in arctic climate are highly correlated with variations in the AO, e.g. through the advection of heat and redistribution of sea ice by the wind (Rigor et al. 2002).

Rigor et al. (2002) show that an AO-related decrease in sea level pressure drove a change towards less anticyclonic sea ice motion over the Arctic, which should have increased the Ekman divergence of sea ice, and also tended to increase the advection of

sea ice away from the coast of the East Siberian and Laptev seas (Fig. 13). These processes should have had the effect of producing more new, thin ice in the coastal flaw leads. This suggests that at least part of the thinning of sea ice noted by Rothrock et al. (1999) is attributable to the trends in the AO towards high-index polarity. Rigor et al. (2002) also show that the spring and autumn surface air temperature and summertime sea ice concentration are all strongly correlated with the AO-index for the previous winter (Fig. 10 right column). These correlations reflect the dynamical influence of the AO on the thickness of the wintertime sea ice, whose persistent "footprint" is reflected in the heat fluxes during the subsequent spring, in the extent of open water during the subsequent summer, and in the heat liberated in the freezing of the open water during the subsequent autumn. These mechanisms are important on the year-to-year and decadal timescales, and the dynamic thinning of sea ice over the past few decades is at least partially responsible for the warming of surface air temperature over the Arctic. Since 1995, the AO-index has averaged near normal. On the basis of the arguments presented in Rigor et al. (2002), sea ice conditions should have returned to near normal during this period, but this has not been the case.

The summers of 1998, 2002, and 2003 set records for low sea ice extent on the Arctic Ocean. The spatial pattern of these recent trends in summer sea ice extent (1979–2002, Fig. 9b) was different from the pattern of trends noted by Parkinson, et al. (1999) for the period 1979–1996 (Fig. 9a). The summer trends for 1979–1996 (Parkinson, et al. 1999) were dominated by large decreases in sea ice extent on the Eurasian side of the

Arctic Ocean, while trends for 1979–2002 were strongest along the Alaskan coast, where the effect of the wintertime AO is less dramatic (Fig. 13).

Anomalous wind patterns during the summers could have contributed to the areal extent of open water along the Alaskan coast. For example, southeasterly wind anomalies should increase the advection of ice away from the Alaskan coast and increase the advection of warm, continental air onto the ocean; both processes act to decrease the amount of sea ice in the Beaufort and Chukchi seas (e.g. Drobot and Maslanik, 2003). However, these processes do not account for the record minima in sea ice extent during the summers of 2002 and 2003, when surface air temperatures along the Alaskan coast were colder than normal and the sea ice drifted towards the Alaskan coast (Serreze et al. 2003). In this dissertation it is argued that the changes in surface wind that occurred in association with the high-index state of the AO during the interval 1989–1995 dramatically decreased the average age of sea ice on the Arctic Ocean, thereby setting the stage for the recent minima in arctic sea ice extent.

This dissertation builds on the work presented in my Masters thesis, which has been published in two papers (Rigor, et al. 2000; and Rigor et al. 2002), and is organized as follows. Section 2 discusses the data sets and methods. Section 3 describes the primary patterns of variability in sea ice concentration, sea ice motion, and temperature advection in order to understand the processes that affect summer sea ice extent using the objective analysis procedures empirical orthogonal function (EOF) analysis and maximum covariance analysis (MCA). Comparison of the EOF and MCA patterns lends insight into the processes that affect summer sea ice extent. In Section 4 a

simple model is used to estimate the age of sea ice as a proxy for sea ice thickness, and these estimates of the age of ice provide a basis for explaining the deviations of sea ice extent from the expected sea ice conditions given the prevailing atmospheric forcing during recent years. And finally, in the concluding section, it is argued that the redistribution of sea ice by the wind (dynamics) plays a more important role than temperature advection (thermodynamics) in the year-to-year variations in summer sea ice extent.

2. Data and Analysis Techniques

The data sets used in this study are sea ice concentration, sea level pressure, temperature advection, and sea ice motion for the 48-year period 1955–002.

a. Sea Ice Concentration and Extent

Sea ice concentration is defined as the fraction of the area of the ocean covered by sea ice. This study uses the sea ice concentration data documented in Walsh (1978), which is available for the period 1901–1999, and in Comiso (1995), which has been updated the include the period of record 1979–2002. The Walsh (1978) data set combines observations from a number of different sources such as navigational ice charts based on aircraft reconnaissance and ship reports, and includes satellite data beginning in the 1970's. The Comiso (1995) data are analyzed from the passive microwave satellite data using the Bootstrap sea ice concentration algorithm. These data were obtained from the EOS Distributed Active Archive Center (DAAC) at the National Snow and Ice Data Center (NSIDC), University of Colorado at Boulder. Here the Walsh (1978) data are used for the period prior to 1979, and the Comiso (1995) data after 1979.

Sea ice extent is defined as comprising the areas with at least 90% sea ice concentration. It should be noted that we use the terms *sea ice concentration* and *sea ice extent* interchangeably because the goal here is to understand the changes in summer sea ice along the coast where the sea ice concentrations tend to be either close to zero or

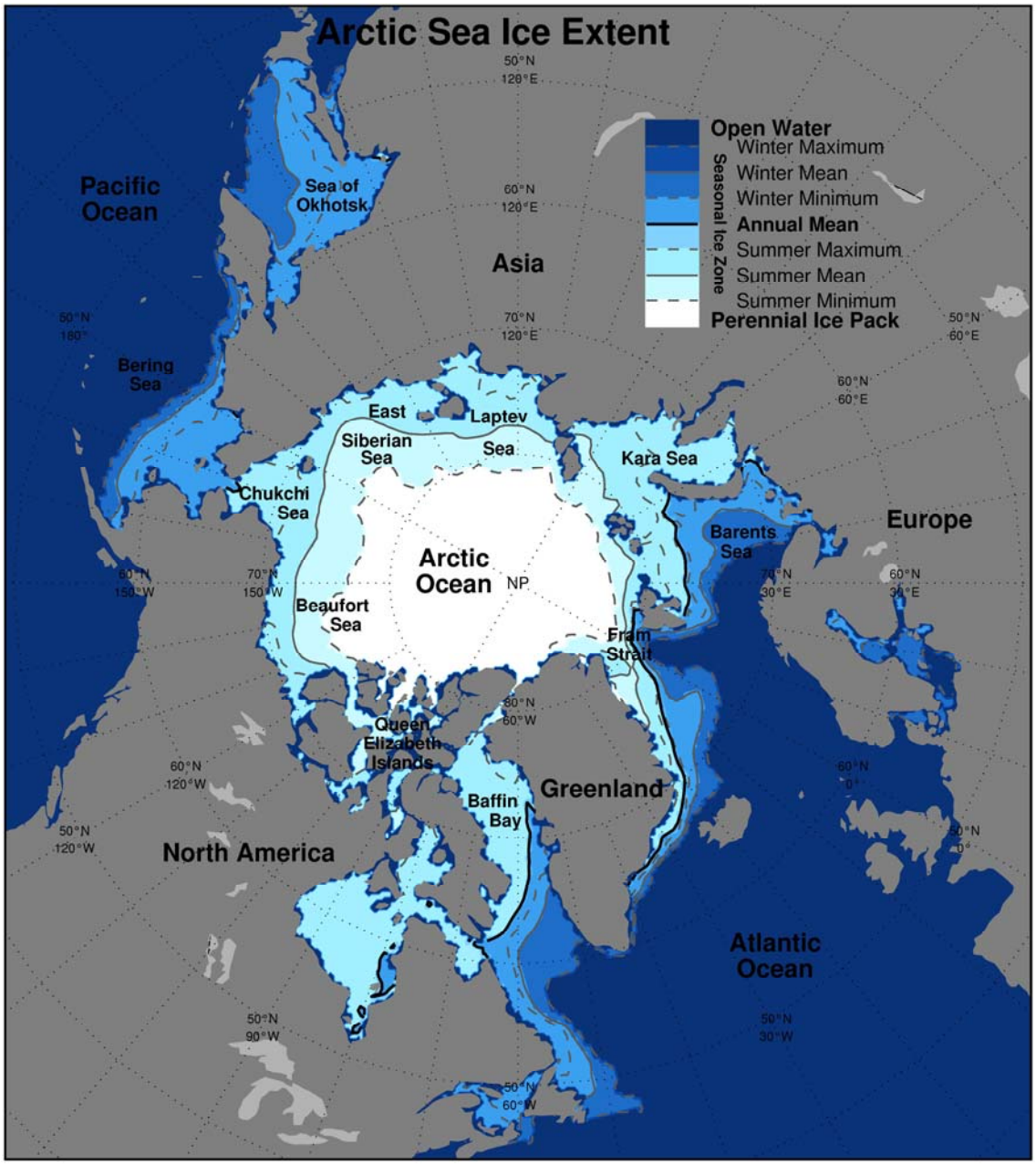

Figure 14. Climatological mean sea ice extent and geography of the Arctic. The seasonal mean sea ice extent lines define the boundary within which sea ice has been observed during at least half the seasons on record (1901–2002), the seasonal minimum lines define the boundary within which sea ice has been observed during all seasons, and seasonal maximum lines define the boundary within which sea ice has been observed at least once.

close to 100%. Sea ice concentration and sea ice extent are highly correlated ($R \approx 0.9$, Deser et al. 2000).

The average extent of sea ice estimated from these data varies from 4.7×10^6 km^2 during summer (Fig. 14), when sea ice in the Arctic is typically only found in the interior of the Arctic Ocean and in the Greenland Sea, to 14.4×10^6 km^2 in winter when ice in the Arctic extends south to cover the Sea of Okhotsk, the northern reaches of the Bering Sea, Baffin Bay, the Labrador Sea, and a part of the North Atlantic. During summer, sea ice extent ranges from 3.3×10^6 km^2 to 7.9×10^6 km^2, and during winter from 13.3×10^6 km^2 to 17.6×10^6 km^2.[†] Figure 14 also shows the geographical locations of areas discussed in this dissertation.

The spatial pattern of trends in sea ice extent varies depending on the period over which the trends are estimated (e.g. Fig. 9). Prior to 1996 the trends in summer sea ice extent were strongest in the Eurasian side of the Arctic Ocean (Fig. 9a), but after 1996 the strongest trends were observed in the Beaufort and Chukchi seas (Fig. 9b). The focus here is to study the year-to-year variations in summer sea ice, with emphasis on the mechanisms forcing these changes. September data are used to represent summer sea ice extent because September is the month of minimum sea ice extent, and hence it represents the cumulative melting that has taken place during the summer season. For

[†] The seasonal mean sea ice extent lines define the boundary within which sea ice has been observed during at least half the seasons on record (1901 – 2002), the seasonal minimum lines define the boundary within which sea ice has been observed during all seasons, and seasonal maximum lines define the boundary within which sea ice has been observed at least once.

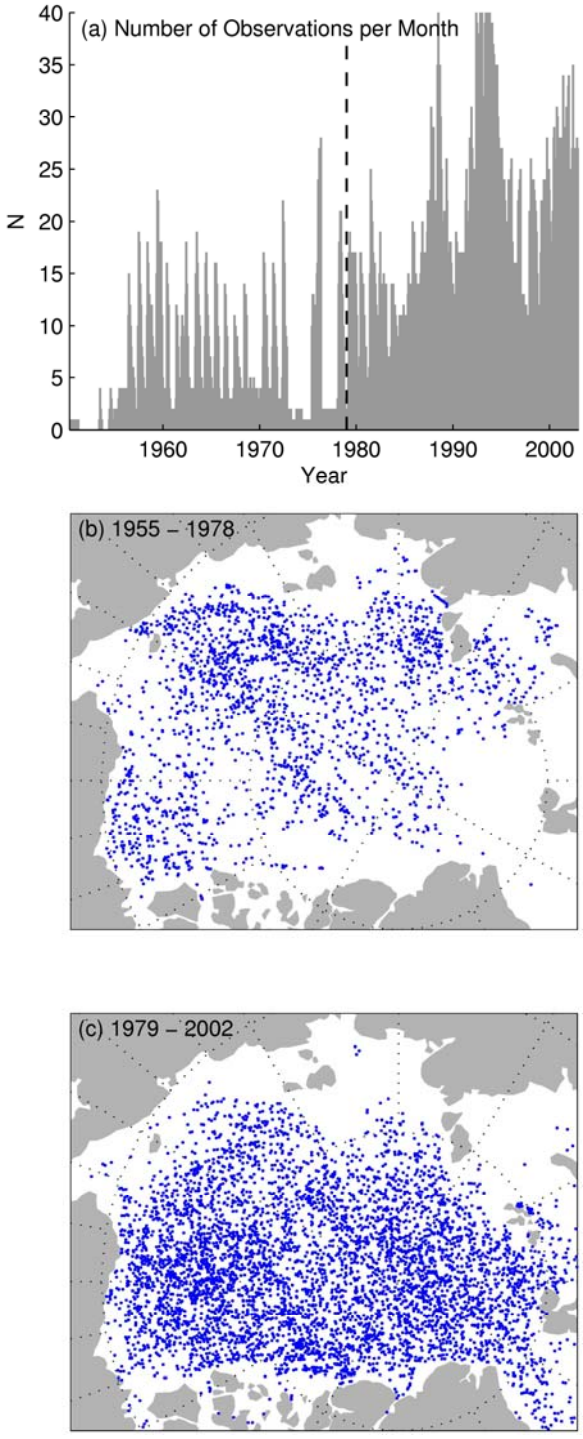

Figure 15. Sea ice motion observations: (a) number for each month; (b) positions from 1955–1978; and (c) positions from 1979–2002.

discussion of the variations in winter sea ice extent, suggested reading include are Partington et al. 2003, Deser et al. 2000, and Fang and Wallace, 1994.

b. Sea Ice Motion

The observed drifts of sea ice were obtained from the International Arctic Buoy Programme (IABP, http://iabp.apl.washington.edu). These data include observations from manned research stations drifting (1955–1991) on the Arctic Ocean, the Russian Drifting Automatic Radiometeorological Stations (DARMS) buoy program (1955–1973), the Arctic Ice Dynamics Joint Experiment (AIDJEX, 1975–1978), and the IABP (1979–2002). Figure 15 shows a) the number of observations available for each month of the record, b) the locations of the 2041 observed drifts from 1955–1978, and c) the locations of the 5825 observations from 1979–2002. Although there were fewer observations prior to the era of the IABP, the data for 1955–1978 provide extensive coverage of the Arctic Ocean. Observations prior to 1955 are also available (e.g. Nansen's ship the *Fram* drifted on the Arctic Ocean from 1893 to 1896), however, continuous observation of ice motion did not begin until mid-1954 with the deployment of the Russian North Pole drifting station NP-3. Thus this study begins in 1955. For the study period (1955–2002), data from 39 manned research stations are available, the bulk (29 stations) of which were collected by the manned research stations of the Russian North Pole (NP) program (1937-1991). The NP data were provided by the Arctic and Antarctic Research Institute (AARI), St. Petersburg. The Russian DARMS buoy program (1953–1972) deployed an average of 11 stations per year throughout the

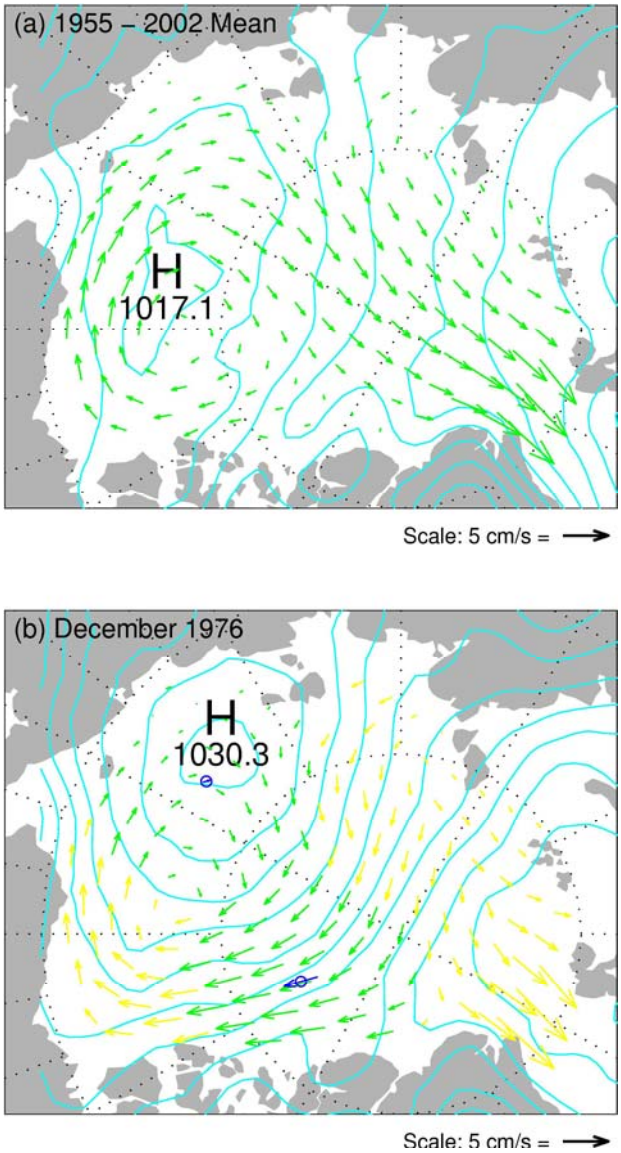

Figure 16. Analyzed fields of sea level pressure and sea ice motion: (a) Climatological mean from 1955–2002. Sea level pressure contours are shown every 1 hPa; and (b) for December 1976. Sea level pressure contours are shown every 2 hPa. The green arrows show. The observed velocities for the drifting stations (NP-22 and NP-23) are shown as a blue vectors with an open circles marking their positions. The green arrows show the analyzed field of sea ice motion where the variance of the error is < 0.5 near the observations, and the yellow arrows show the estimated sea ice motion where the variance of the error is ≥ 0.5, over 700 km from the observation.

Russian Marginal Seas. Typically the number of DARMS buoys was ~15 after the spring deployments and an average of 9 in late winter. The AIDJEX program (1972–1976) deployed 4 ice stations and 43 buoys. The IABP began deploying buoys in 1979, greatly increasing the number of concurrent observations of sea ice motion. Data from over 500 buoys were used, and on average ~25 IABP buoys were reporting at any given time.

The monthly gridded fields of sea ice motion were calculated from the displacements of the observations during each month following the optimal interpolation (OI) scheme described in Rigor et al. (2002) in which different measurement errors are specified for different types of observations. These errors depend on the methods used to position the stations (e.g. satellite Doppler positioning and radio triangulation) and range from 300 m to over 25 km. The velocity errors range from less than 0.02 cm/s for IABP buoys to as high as 0.7 cm/s for AIDJEX and DARMS buoys. Although the latter values are relatively high compared to the mean monthly ice motion (3–4 cm/s), these data are of sufficient accuracy to be useful in the optimal analysis, which simply applies less weight to the observations with higher measurement errors. The OI analysis also provides an estimate of the standardized variance of the error. It should be noted that optimal interpolation analysis biases its estimate towards the "first guess field" which is, in this case, the climatological mean field of sea ice motion (Fig. 16a). In areas of sparse data where the estimated error is high (> 0.5 in dimensionless units), the analysis essentially returns the value of the climatological mean field of ice motion. As noted earlier, the drift of sea ice is driven by

the winds and ocean currents. The mean field of ice motion shows many typical features of arctic sea ice motion such as its primarily wind driven motion in the Beaufort Gyre and its cross-isobar flow in the Transpolar Drift Stream.[♦]

The analyzed sea ice motion and sea level pressure fields for December 1976 are shown in Fig. 16b. The observed velocities for the drifting stations (NP-22 and NP-23) are shown as blue vectors with open circles marking their positions. The green arrows show the analyzed field of sea ice motion where the variance of the error is < 0.5 near the observations, and the yellow arrows show the estimated sea ice motion where the variance of the error is ≥ 0.5, over 700 km from the observation. The analyzed sea ice motion field for December 1976 (Fig. 16b) assimilates the deviations from the climatological mean field of sea ice motion determined by the observations. The consistency between the sea ice motion vectors and the sea level pressure field shown in Fig. 16b suggests that although there were at times only 1 or 2 stations drifting on the Arctic Ocean prior to 1979 (Fig. 15a), given the long correlation length scale between observations of ice motion of 1300 km (Pfirman et al. 1997), the estimated fields of sea ice motion for 1955–2002 are reliable. In the area of the high in sea level pressure sea ice motion is slower than the mean because the winds (pressure gradients) are weaker, while north of the Canadian Archipelago the winds are stronger and thus the sea ice motion in the area is faster. Further verification of the sea ice motion fields from 1955 to 1978 is presented in Appendix B.

[♦] The Transpolar Drift Stream is the zone of faster moving sea ice drifting Eurasian side of the Arctic Ocean, across the North Pole towards Fram Strait. See Fig. 14 for geographic locations.

c. NCEP Reanalysis Sea Level Pressure and Temperature Advection

The sea level pressure, wind, and air temperature data used in this study are the National Center for Environmental Prediction–National Center for Atmospheric Research (NCEP-NCAR) reanalysis (Kalnay et al. 1996). The wind and temperature data were used to estimate the horizontal temperature advection and subsidence (adiabatic warming) at 925 hPa. These data are available for the period 1948–2002. In order to show the cumulative effects of the changes in atmospheric circulation on summer sea ice, the mean of December–March, and June–August is used to represent winter and summer conditions, respectively.

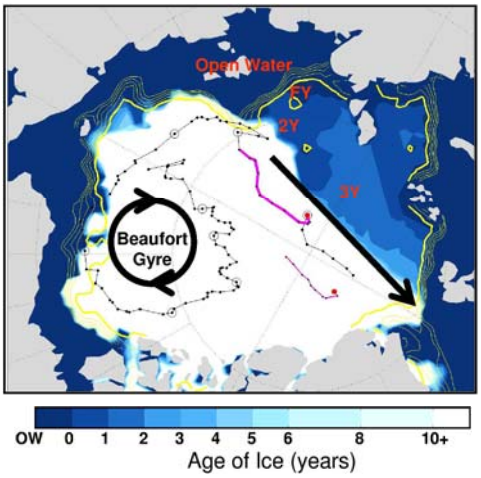

Figure 17. Age of oldest sea ice in September 1981 based on the simulation. Open water (OW) is shown as dark blue, and the oldest ice is shown as white. The drift of buoys that reported for at least 8 months of the prior 12 months are also shown (magenta lines with black dots), with a large red dot marking the current position. Tracks without large red dots mark buoys that have ceased reporting. The thick yellow line marks 90% ice concentration, while the thinner yellow lines mark sea ice concentrations of 50, 60, 70, and 80% for those months as inferred from the Walsh (1978) and Comiso (1995) data sets. Figure a also shows the drift of the Russian manned drifting station, NP-22, from 1973 to 1982 (black trajectory), with dots marking monthly positions, and circles noting the position of the station during September of each year; and areas of open water, first (FY), second (2Y), and third year (3Y) ice are noted in red. The center of the Beaufort Gyre (BG) and Transpolar Drift Stream (red arrow) are also shown.

d. Age of Sea Ice Model

As a proxy for sea ice thickness, we estimate the age of sea ice on the Arctic Ocean is estimated using a simple model that (1) advects parcels of ice using monthly gridded fields of ice motion, (2) forms new, first year sea ice in the areas of open water that develop wherever multi-year ice is advected away from the coasts, and (3) keeps track of the age of the ice that survives the summer melt. The age of the sea ice is increased by one year at all grid points that lie within the 90% sea ice concentration limit in September of that year. The model was initialized by assuming that all of the

sea ice surviving the summer melt in 1955 was 1 year old, so that by model year 1965 the distribution of the ice ranging in age from 0–10 years is well established. Figure 17a shows the estimated age of ice on the Arctic Ocean in September 1981. Throughout most of the Arctic Ocean the ice is over 10 years old. This estimate is consistent with the drift of the Russian manned drifting station NP-22, which was deployed in the Beaufort Gyre in 1973 on thick multi-year ice and abandoned nearly 10 years later in 1982 as it drifted towards Fram Strait (Fig. 17), and by the drift of T-3, which remained confined within the Arctic Ocean for over 30 years from 1952–1983 (not shown). Younger ice can also be seen in the Transpolar Drift Stream (black arrow), which quickly advects sea ice across the Arctic Ocean towards Fram Strait. Estimates of the age of ice derived from the model are used to show how the changes in age are related to thickness, and the changes in summer sea ice extent.

e. Sea Ice Thickness

Estimates of sea ice thickness from satellite altimeters, submarine upward looking sonars, and a coupled ocean–ice model were used to validate the age of sea ice model. The sea ice thickness climatology estimated from the ERS-1 and ERS-2 satellite altimeter data were provided by S. Laxon and are documented in Laxon et al. (2003). The submarine sea ice draft data from 1986 to 1998 were obtained from the NSIDC. The coupled ocean–ice model data were provided by J. Zhang and are documented in Zhang and Rothrock (2003).

f. Methods

The primary goal of this dissertation is to understand the variability of summer sea ice extent, and how this variability is driven by changes in wind and temperature over the Arctic Ocean. To do this, empirical orthogonal function (EOF) analysis is used to identify the primary modes of variability of these data sets, and maximal covariance analysis (MCA) to identify the primary modes of covariability between these data sets (Bretherton et al., 1992). These procedures are widely used in the analysis of climate data, and take advantage of eigenvector analysis and singular value decomposition, standard techniques of linear algebra that transform a space/time data matrix to a set of vectors (i.e., time series comprised linear combinations of the original time series). The set of vectors is usually truncated: the leading ones that explain most of the variance in the original matrix are retained and the remaining ones are discarded. EOF analysis and MCA are forms of Fourier analysis, which is also used to transform a space-time field into coefficients of a prescribed set of analytic functions such as sines and cosines or spherical harmonics. Expansions involving analytic functions are often truncated, retaining just the modes corresponding to a prescribed range of spatial scales or the modes that capture most of the variability in the original space/time field. Ideally the modes derived from Fourier analysis can be attributed to physical processes, but this is not always the case.

In EOF analysis the leading modes account for the maximal fraction of the variance in a single dataset and in MCA the leading modes account for the maximal

fraction of the squared covariance between the time series in a pair of datasets. Both methods yield three products relating to a set of "modes": (1) a scalar that describes the relative prominence of the mode in terms of variance (for EOF's) or covariance (for MCA), (2) spatial patterns (a single pattern for EOF analysis and a pair of patterns for MCA, one for the left field and one for the right field), and (3) time series describing variations in the amplitude and polarity of the pattern (a single series for EOF's and a pair of series for MCA, one for the left field and one for the right field). In EOF analysis both the spatial patterns and their associated time series are mutually orthogonal; in MCA only the spatial patterns are orthogonal. The two MCA time series represent the relative temporal strength of their respective spatial modes in the original data, i.e., although the paired modes are highly correlated, the individual variability of these modes within their respective data sets may differ from the other over time. For example, Drobot and Maslanik (2003) show that decreases in summer sea ice extent in the Beaufort Sea may be attributed to southeasterly wind anomalies, which should increase the advection of ice away from the Alaskan coast and increase the advection of warm, continental air onto the ocean. However, record minima in sea ice extent were observed during the summers of 2002 and 2003, when surface air temperatures along the Alaskan coast were colder than normal and the sea ice drifted towards the Alaskan coast (Serreze et al. 2003). In this case, MCA analysis between summer sea level pressure and sea ice extent should produce spatial patterns in which exhibit southeasterly winds that coincide with areas of lower sea ice extent, and a strong

coherence between the two MCA time series over most of the record, which should decrease during 2002 and 2003.

In this study EOF analysis is performed by singular value decomposition of the space/time anomaly matrix of each of the datasets, where the grid point values are area weighted by the square root of the cosine of latitude. This procedure yields the principal component time series (PC), and the EOFs (spatial patterns) for each mode of variability. MCA is performed by singular value decomposition of the temporal covariance matrix between the area weighted anomalies of two datasets. The left and right matrices produced by the MCA analysis represent the singular vectors (spatial patterns) of the modes of covariability between two data sets, i.e. two spatial maps for each mode are produced, one from the left matrix and one from the right matrix. These paired maps represent the primary modes of variability in one data set that are most highly correlated with a mode of variability in the second data set. The expansion coefficient time series (EC) for each map in pair are estimated by projecting the area weighted anomalies onto the singular vectors. The singular values provide an estimate of the squared covariance fraction explained by each mode; these values are shown in the upper right corner of the figures (Fig. 18-22). All EOF and MCA modes shown are well separated (statistically independent modes) according to the criterion of North et al. (1982) unless noted otherwise in the text. All regression maps are estimated by regressing the original data sets on standardized time series so the maps may be interpreted as anomalies (in units of the original data) per standard deviation of the associated indices.

3. Patterns of Variability

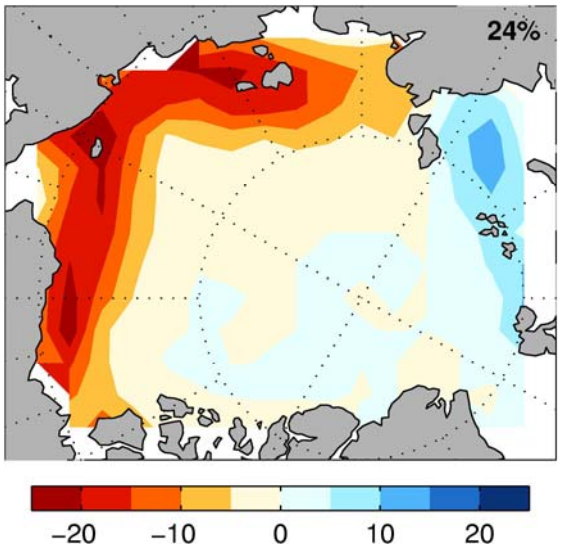

Figure 18. Regression map of sea ice concentration on the first PC of September sea ice concentration for 1955–2002. (Units: %/SD of PC).

In this section we investigate the primary patterns of variability in September sea ice concentration, and study to roles of sea ice motion and temperature advection in forcing this variability.

a. Variations in September Sea ice Extent

Figure 18 shows the first EOF of September sea ice concentration, which exhibits a strong center of action extending from the Laptev Sea to the Beaufort Sea. This pattern is qualitatively similar to the observed trends in September sea ice concentration (Fig. 9), however, the trends from 1979 to 1996 are stronger in the East Siberian Sea, while the trends from 1979 to 2002 are more pronounced in the Chukchi

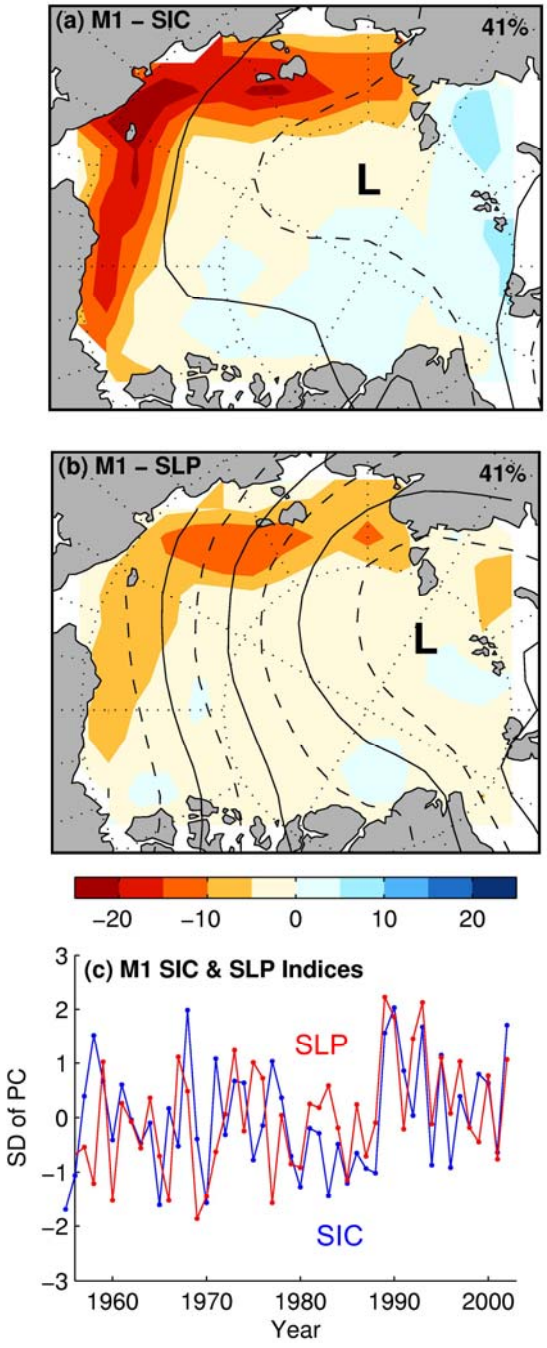

Figure 19. Regression maps of September sea ice concentration and wintertime (DJFM) sea level pressure (70–90°N) on the first EC time series of September sea ice concentration (a, and blue line in c), and previous wintertime sea level pressure (b, and red line in c) obtained from the MCA of September sea ice concentration and previous wintertime sea level pressure (Units: % and hPa per SD of the EC time series). Solid contours are shown every 1 hPa.

and Beaufort seas.

To identify the primary atmospheric circulation patterns associated these changes in summer sea ice concentration an MCA analysis was performed between September sea ice concentration and sea level pressure the previous winter (DJFM) and summer (JJA). Figure 19 shows the sea ice concentration and sea level pressure fields obtained by regressing those fields upon (a) the sea ice concentration EC time series, and (b) the sea level pressure EC time series obtained from MCA. These maps exhibit a strong sea level pressure center of action in the Eurasian Arctic. In contrast to the pattern in the leading EOF of September sea ice concentration (Fig. 18), the sea ice concentration anomalies in the East Siberian and Laptev seas are stronger than the anomalies in the Beaufort and Chukchi seas. In Rigor et al. (2002) this mode was interpreted as representing the year-to-year variability in the production of new sea ice during winter driven by variations in wind associated with the wintertime AO. The EC time series of wintertime sea level pressure obtained from the MCA of September sea ice concentration and previous wintertime sea level pressure (Fig. 19c) is highly correlated with the wintertime AO index [R(sea level pressure EC time series, AO) = 0.91].

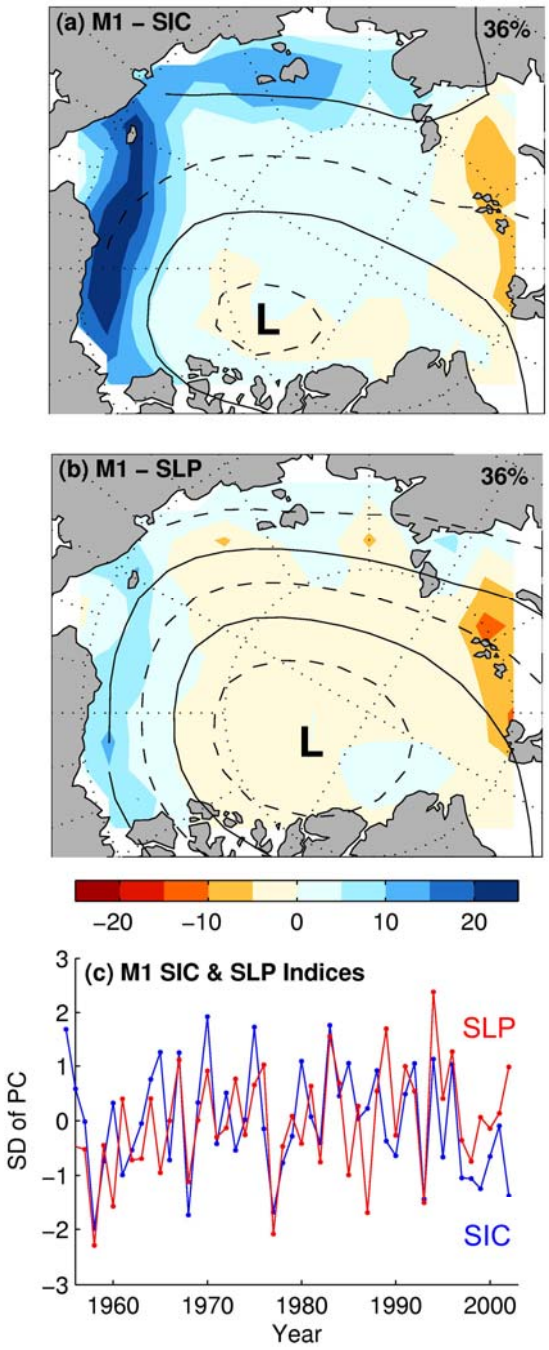

Figure 20. Regression maps of September sea ice concentration and summer (JJA) sea level pressure (70–90°N) on the first EC time series of September sea ice concentration (a, and blue line in c), and summer sea level pressure (b, and red line in c) obtained from the MCA of sea ice concentration and sea level pressure (Units: % and hPa per SD of the EC time series). Solid contours are shown every 1 hPa.

The corresponding maps based on MCA between September sea ice concentration and summer (JJA) sea level pressure are shown in Fig. 20. These maps show sea ice concentration anomalies that are stronger in the Beaufort and Chukchi seas than in the East Siberian and Laptev seas. This pattern has been related to changes in summer circulation (e.g. Drobot and Maslanik, 2003) and resembles the record minima in summer sea ice extent during three of the past six summers (Fig 9b). The EC time series (Fig. 20c) is highly correlated with the summertime AO [R(sea level pressure EC time series, AO_{JJA}) = –0.93].

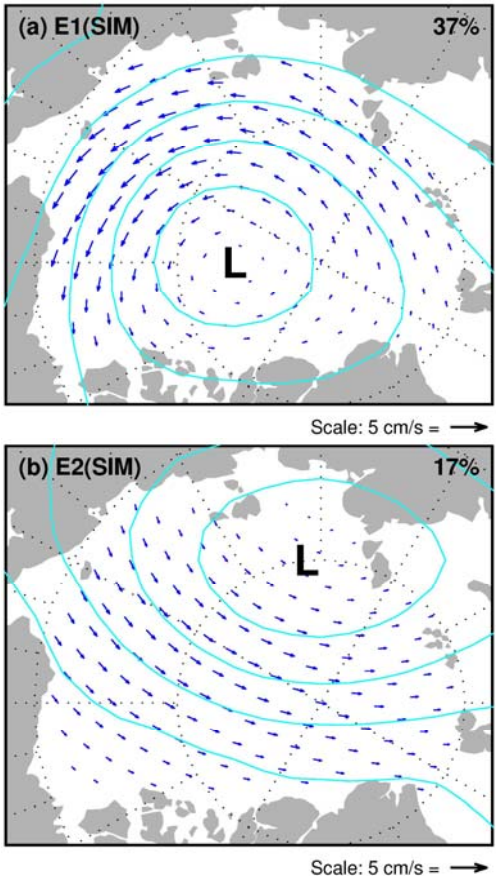

Figure 21. Regression maps of sea ice motion and sea level pressure on the first two PCs of sea ice motion for all months for 1955–2002. The variance fraction explained by each PC is shown in the upper right corner of each map. Units are hPa and cm/s per standard deviation of the PCs. Contours are shown every 1 hPa.

b. Variations in Sea Ice Motion and Sea Level Pressure

The primary patterns of variability of summer sea ice concentration are related to changes in atmospheric circulation related the variations in AO conditions. Are these changes in summer sea ice concentration due to the redistribution of sea ice or the advection of heat onto the Arctic Ocean by the winds?

The drift of sea ice is primarily forced by the winds and ocean currents (e.g. Hibler, 1986; and Thorndike, 1989). On time scales of days to years, the winds explain most of the variance in sea ice motion. For example, Thorndike and Colony (1982) show that the variations in the winds explain over 70% of the day-to-day variance, and on longer time scales of seasons to years, Rigor et al. (2002) show that the month-to-month variations in sea ice motion are strongly influenced by variations in wind associated with the AO.

Figure 21 shows the first two EOFs of sea ice motion from 70°N to 90°N for all months from 1955 to 2002. Also shown are fields of sea level pressure regressed on the PCs of sea ice motion. The first EOF (Fig. 21a) shows an AO–lke structure in the sea level pressure field with a dominant center of action over the central Arctic Ocean and sea ice motion anomalies circulating around that center in the same sense as the geostrophic surface wind anomalies as inferred from the sea level pressure anomalies.

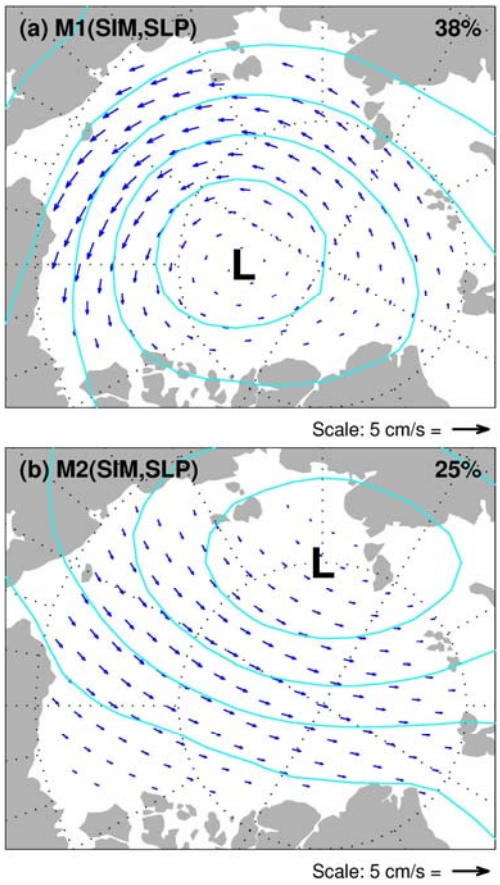

Figure 22. Regression maps of sea ice motion and sea level pressure on the first twoa ice motion EC time series of the MCA of sea ice motion and sea level pressure (70–90°N) for all months of 1955–2002. The covariance fraction explained by each EC time series is shown in the upper right corner of each map. Contours are shown every 1 hPa.

The second EOF of sea ice motion consists of a transpolar flow with a dominant center of action over the Laptev Sea. For the polarity shown, with negative sea level pressure anomalies over the Laptev Sea, the anomalous sea ice motions produce an anomalous advection of sea ice away from the East Siberian and Alaskan side of the Arctic Ocean, over the North Pole, towards Fram Strait and the Barents Sea. This pattern is similar to the sea level pressure field that Holland (2003) associated with winter-to-winter variations in Fram Strait ice export (see his Fig. 14).

Figure 22 shows the fields of sea ice motion and sea level pressure obtained by regressing these fields upon the first two sea ice motion expansion coefficient (EC) time series obtained from MCA of sea ice motion and sea level pressure. These patterns resemble the EOFs of sea ice motion. The first EC time series of sea level pressure is highly correlated with the AO (R = 0.84). The second MCA mode shows the cross arctic flow associated with an increase in ice flux through Fram Strait and into the Barents Sea (Holland, 2003). The regression maps based on the sea level pressure EC time series (not shown) are qualitatively similar, but as expected (Wallace, et al. 1992), the sea level pressure features are stronger and the sea ice motion features weaker than shown in the regression maps on the sea ice motion EC time series (Fig. 22). These results agree with past studies of sea ice motion (e.g. Rigor et al., 2002) which show that most of the variability in sea ice motion is related to changes in wind (i.e. the first two EOF's of sea ice motion fields explain 37% and 17% of the variance of sea ice motion, respectively, and are associated with the first two EOF's of the sea level pressure fields).

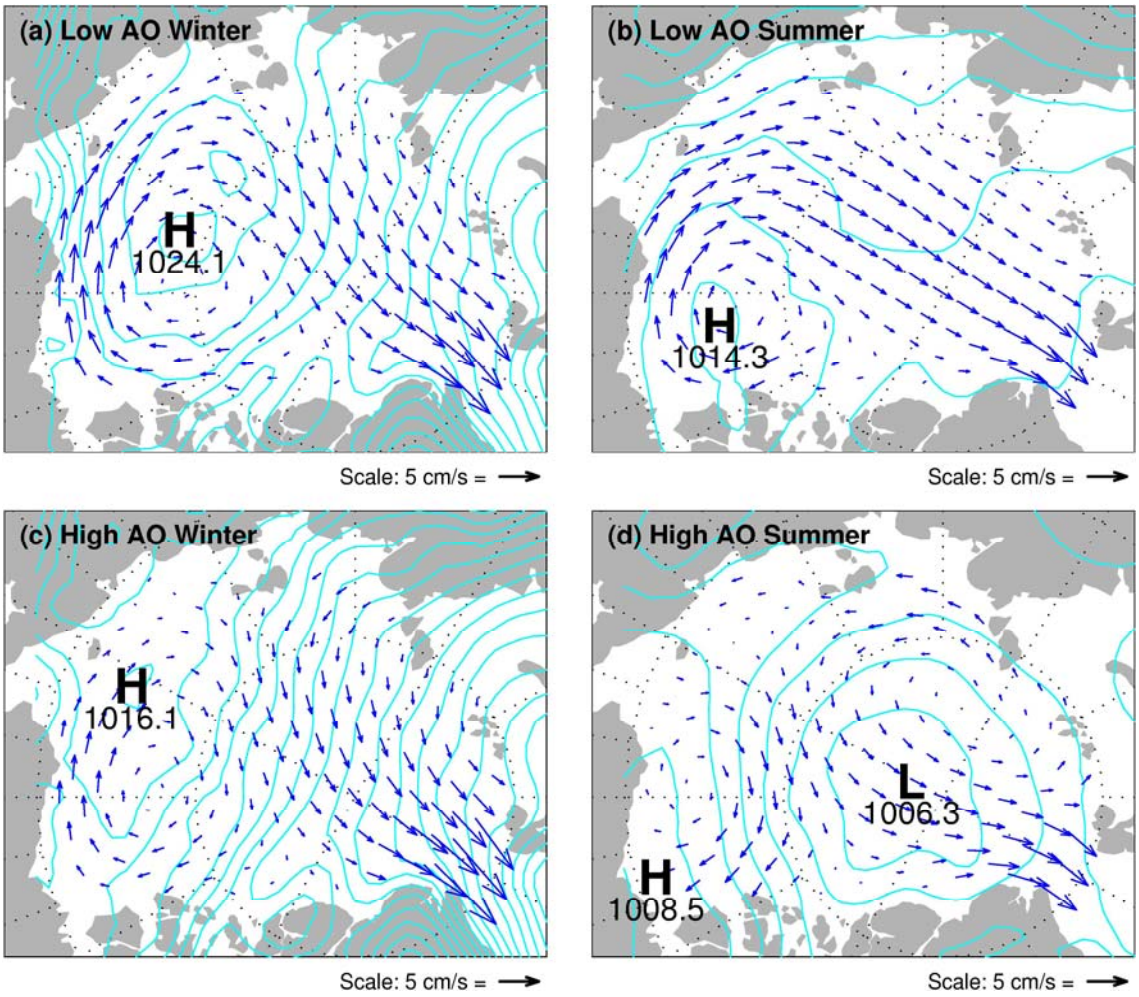

Figure 23. Composite maps of AO sea level pressure and sea ice motion: (left) winter, (right) summer, (top) low index, and (bottom) high index.

The impact of the AO upon summer sea ice extent through the redistribution of sea ice during winter and summer can be inferred from the sea ice motion fields. Figure 23 shows the sea ice motion and sea level pressure fields for high and low AO conditions during winter and summer. These maps are qualitatively similar to the maps shown in Rigor et al. (2002, their Fig. 9), but are for the extended period 1955–2002. During low AO conditions these maps show:

1) the Beaufort Gyre is stronger and covers most of the Arctic Ocean
2) sea ice in the larger gyre tends to get packed into the East Siberian Sea
3) the Transpolar Drift Stream is shifted towards the Eurasian side of the Arctic, drawing ice primarily from the Laptev Sea

During neutral (not shown) to high AO conditions (Fig 23. bottom):

1) the Beaufort Gyre is weaker and confined to the Beaufort Sea
2) there is a net export of sea ice from the East Siberian Sea
3) the Transpolar Drift Stream is shifted westward towards the Alaskan and the Canadian Archipelago, and draws ice from both the Laptev and East Siberian seas

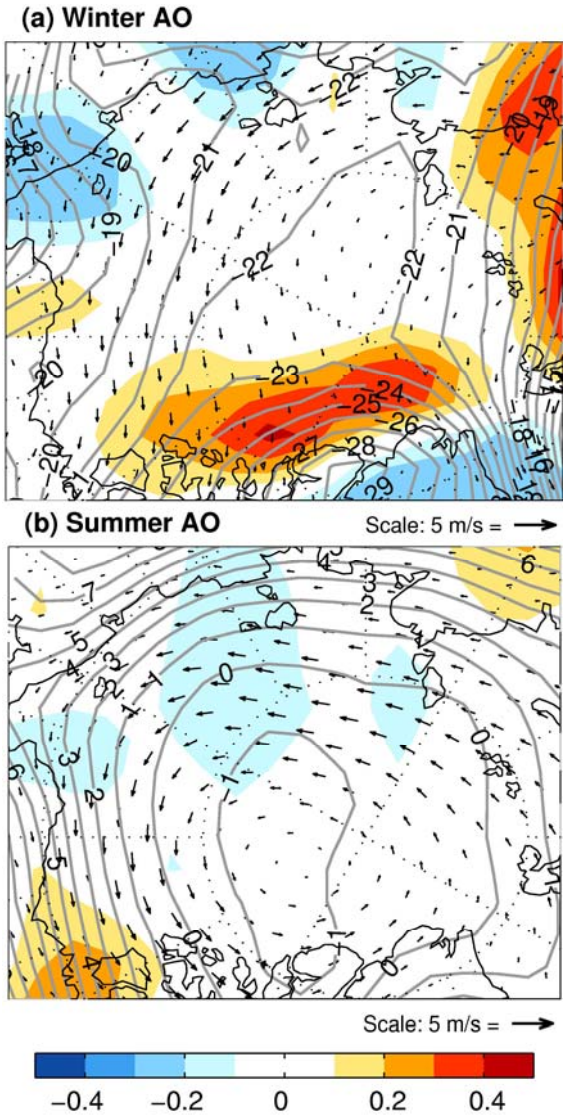

Figure 24. Regression maps of (925 hPa) winds (vectors), temperature (contours), and temperature advection (color shading; units: °C/day) on the standardized AO index for winter (a) and summer (b).

c. Variations in the Advection of Temperature onto the Arctic Ocean

The impact of the AO upon summer sea ice extent through the advection of temperature by the anomalous wind field onto the Arctic Ocean during winter and summer is assessed by regressing the seasonal averaged temperature advection fields upon the winter and summer seasonal mean AO indices.[♦] The resulting winter and summer patterns are indicated by colored shading in Fig. 24. Most of the structure in these patterns can be interpreted as a response to the anomalous AO-wind field in the presence of the climatological mean temperature field as indicated by the vectors and contours in Fig. 24.

The patterns shown in Fig. 24a indicate patches of anomalous cold advection during winter over the areas of negative sea ice extent anomalies in the Eurasian Arctic (Fig. 20). If the anomalies in sea ice extent were a local thermodynamic response to surface air temperature, one would expect to observe negative sea ice where the surface air temperature is warm. From a Lagrangian perspective the presence of cold advection along the Eurasian coast indicates that air parcels warm as they pass over regions of negative sea ice anomalies.

The variability of summer sea ice concentration is also affected by summer AO conditions (Fig. 20). High-index AO conditions favor anomalous cold advection during summer over most of the Arctic Ocean (Fig. 24b), however, over the Beaufort and Chukchi seas where the sea ice concentration anomalies related to this pattern are

[♦] Horizontal temperature advection is estimated from the NCEP/NCAR reanalysis wind and temperature data centered at the 925 hPa level, which is 75 hPa deep.

strongest, the influence of the advection of temperature on the ocean is weak and of mixed sign (compare Figs. 20 and 24b). In the Chukchi Sea, weak cold advection is found and in the Beaufort Sea warm advection is apparent over the areas of increasing sea ice concentration.

d. Discussion of Sea Ice Motion and Temperature

The primary modes of variability of sea ice concentration and extent are related to winter and summer AO conditions (Figs 20–22). These results agree with earlier studies reporting that variations in sea ice extent are driven by large–scale variations in atmospheric circulation (e.g. Fang and Wallace, 1994; Shy and Walsh, 1996; Honda et al., 1999; Deser et al., 2000; Zhang et al., 2000; Rigor et al. 2002).

The winter wind anomalies associated with the high-index AO conditions favor anomalous cold advection onto the Eurasian sector of the Arctic Ocean (Fig. 24a), but also favor anomalous advection of ice away from the Eurasian and Alaskan coasts (Fig. 23c). Hence, observed negative anomalies in summer sea ice extent along the Eurasian and Alaskan coasts during the subsequent summers could be dynamically induced; i.e., anomalous advection of ice away from the coast increases the production of thin ice in the flaw leads along the coast, and preconditions the sea ice to be more prone to melt during the following spring and summer. The wintertime pattern of anomalous temperature advection shown in Fig. 24a supports the hypothesis of Rigor et al. (2002) that the trends in summer sea ice extent noted in this area are initiated primarily by the dynamic thinning of sea ice during the previous winter. The lagged regressions between

summer sea ice extent and the previous winter AO also agree with modeling studies (e.g. Bitz, 1997; Walsh and Zwally, 1990), which support the notion that ice thickness during summer in the Siberian Arctic is preconditioned by wintertime conditions.

Low–index AO conditions during summer favor southeasterly wind anomalies, which increase the advection of ice away from the Alaskan coast (Fig. 23b). The influence of the anomalous advection of temperature on the ocean is weak and of mixed sign (Fig. 24b), i.e., warm advection is apparent on the western flank of the decrease in sea ice concentration, however, slight cold advection is apparent on the eastern flank. The lack of a strong pattern in the temperature advection suggests that the advection of ice away from the coast is primarily responsible for the observed negative correlation between the summertime AO-index and summer sea ice extent, which prevails not only in the Chukchi Sea, but along the entire north coast of Alaska.

Given that the regions of negative sea ice anomalies along the Eurasian coast are characterized by cold advection during winter and weak temperature advection during summer, we conclude that the primary cause of the year-to-year variability of summer sea ice concentration and extent in this region is the redistribution of sea ice driven by variations in the wind.

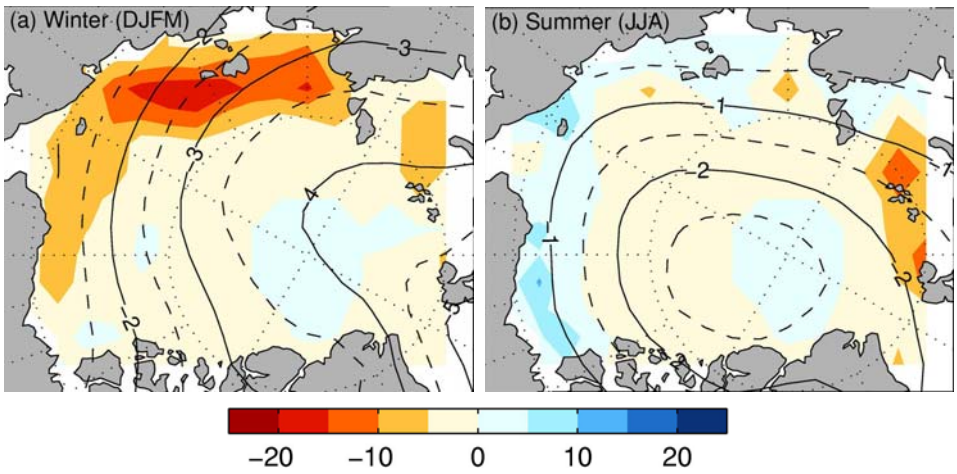

Figure 25. Regression maps of September sea ice concentration and seasonal mean sea level pressure (70–90°N) on (a) the winter mean AO index, and (b) the summer (JJA) mean AO index. (Units: % and hPa per SD of the EC time series). Solid contours are shown every 1 hPa.

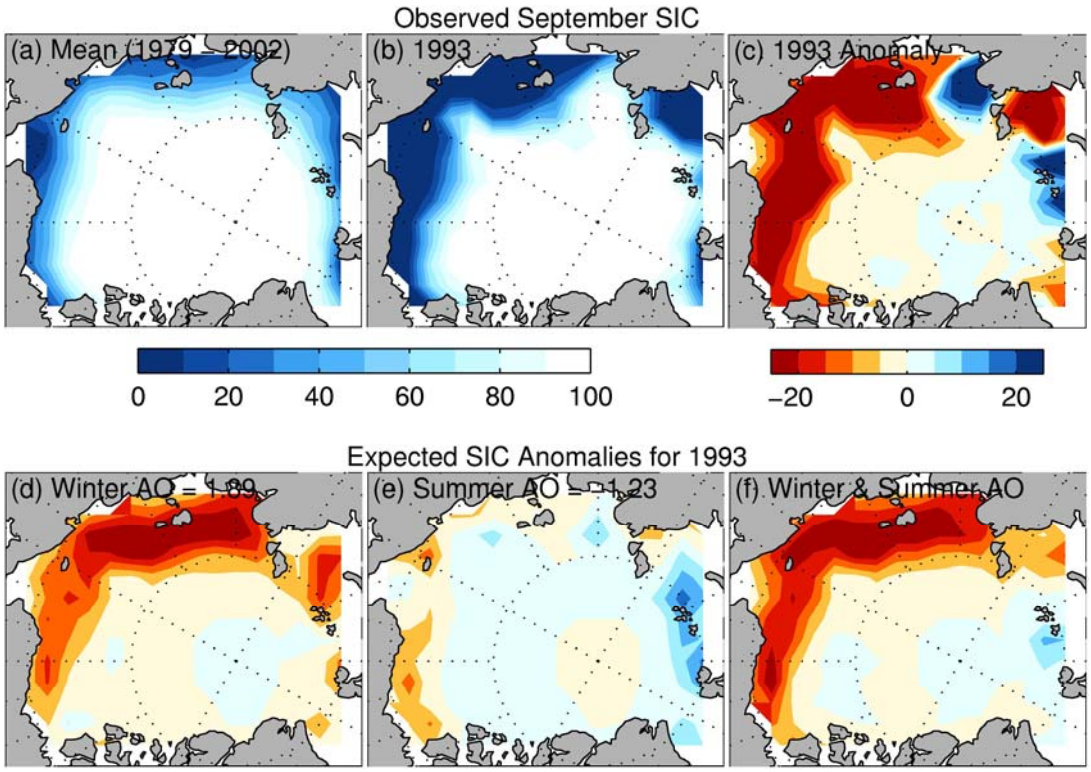

Figure 26. Observed and expected September SIC. The top row shows the (a) climatological mean, (b) observed September 1993 SIC, (c) observed 1993 anomaly, (d) expected based on AO conditions during the prior winter, (e) expected based on AO conditions during summer, and (f) combined prior winter and summer.

e. Variance of September Sea Ice Extent Explained by the Prior Winter and Summer AO Conditions

How much of the variance in September sea ice extent is explained by the prior winter and summer AO conditions? The expected September sea ice extent based on the prior winter and summer AO conditions may be constructed by simply adding an expected anomaly field for each year to the climatological mean field of sea ice concentration (1955–2002). The expected anomaly field for each year may be determined from the regression map of sea ice concentration on the AO index for each season (Fig. 25), multiplied by the value of the AO index for that year. For example, Figs. 26 a–c show the climatological mean field of sea ice concentration, the observed sea ice concentration field for September 1993, and the anomaly from the climatological mean of the September 1993 sea ice concentration field.

Figure 26d shows the expected anomaly in sea ice concentration for September 1993 based on the prior winter AO conditions; this map was constructed by multiplying the regression field shown in Fig. 25a by the standardized anomaly in the AO index for that particular December–March winter season, which was +1.89. Similarly, the expected anomaly based on the summer (June–August) AO conditions (AO_{JJA} = -1.23) is shown in Fig. 26e, and the expected anomaly based on both the prior winter and summer AO conditions is shown in Fig. 26f. These figures show that the basic pattern of the observed anomaly in September 1993 (Fig. 26c) may have been expected by simply knowing the prior winter AO conditions (Fig. 26d). And by monitoring the AO

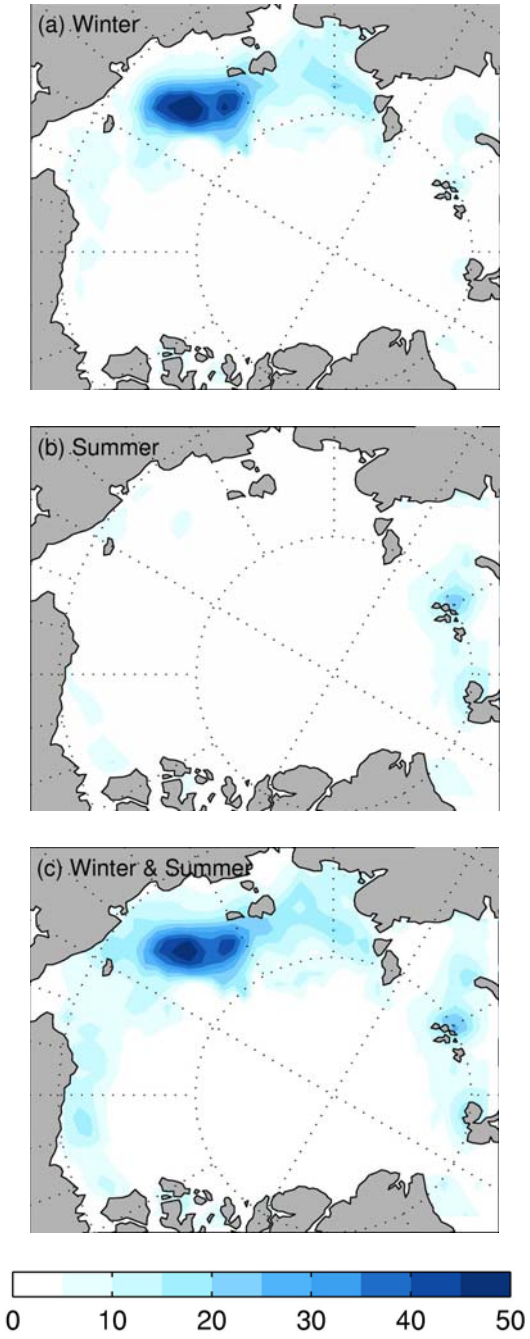

Figure 27. Percent of variance of September sea ice extent explained by the prior winter and summer AO conditions.

conditions through summer, the anomaly would have been expected to intensify along the Alaskan coast (Fig. 26e). Taken together, this simple model reproduces the basic pattern of the observed September 1993 anomaly (compare Figs. 26c and 26f).

Figure 27 shows the percent variance explained of September sea ice extent by the prior winter, prior summer, and prior winter and summer AO conditions combined. The expected September sea ice concentration based on the prior winter AO conditions explain up to 50% of the variance over parts of the Eurasian Arctic. The expected September sea ice concentration based on the summer AO index explains less than 5% of the variance in the Beaufort Sea, and by using both the prior winter and summer AO conditions, the variance explained in the Beaufort Sea is still less than 15%.

These estimates are lower than reported in studies of summer sea ice variability in the Beaufort and Chukchi seas by Drobot and Maslanik (2003) and Maslanik et al. (1999). This discrepancy may be explained by inspection of the EC time series obtained from the MCA of summer sea ice concentration and sea level pressure field (Fig. 20c), which shows that while there were intervals during which the summer atmospheric conditions were highly correlated with the variations in sea ice, there are intervals in which this correlation was weak. For example, there are deviations between EC time series beginning in 1997, and in 2002 the AO index was in a positive phase, which usually favors above normal ice concentrations along the Alaskan coast, and yet record low sea ice extent was observed in the Beaufort and Chukchi seas.

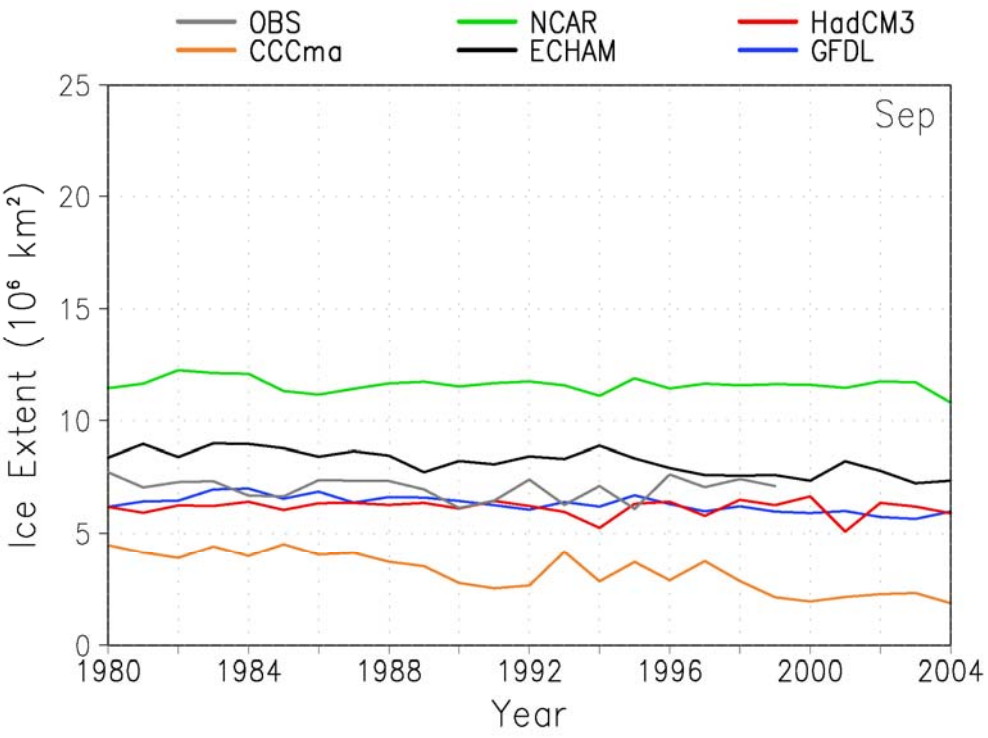

Figure 28. Time series of September sea ice extent simulated by five global climate models. Note the wide range in summer sea ice extent simulated by the different models. The observed sea ice extent is also shown (grey line). Figure provided by M. Timlin and was adapted from Walsh and Timlin, 2003.

4. Variations in the Age of Sea Ice and Summer Sea Ice Extent

The changes in sea ice motion and sea ice extent are related to variations in the AO index during the previous winter and also summer. But the minima in September sea ice extent during the summers of 2002 and 2003 deviate from what would be expected on the basis of these correlations (Fig. 20c). For example, high AO conditions prevailed during the summers of 2002 and 2003, which would favor higher than normal sea ice extent, yet record minima in sea ice extent were observed. Next the investigation is focused on the role of changes in the average age (thickness) of sea ice in accounting for the year-to-year variability of summer sea ice extent. Because the observations of sea ice thickness are sparse in space and time, and global climate models fail to simulate the present day extent of sea ice (Walsh and Timlin, 2003; Fig. 28), the simple model described in Section 2d is used to estimate the age of sea ice as a proxy for sea ice thickness. The age of sea ice can be estimated from observations using the analyzed fields of sea ice motion derived from the drift buoys and manned drifting stations, and observations of sea ice extent (Comiso, 1995; Walsh and Chapman, 1996) The assumption that the thickness of sea ice increases with the age of the ice is supported by the theoretical thermodynamic growth of sea ice; although new sea ice may grow to over one meter thick during its first year, it may not attain its thermodynamic equilibrium thickness under uniform climatic conditions for at least 8 years (Fig. 29; Doronin and Kheisin, 1977). Under more realistic conditions, the thermodynamic

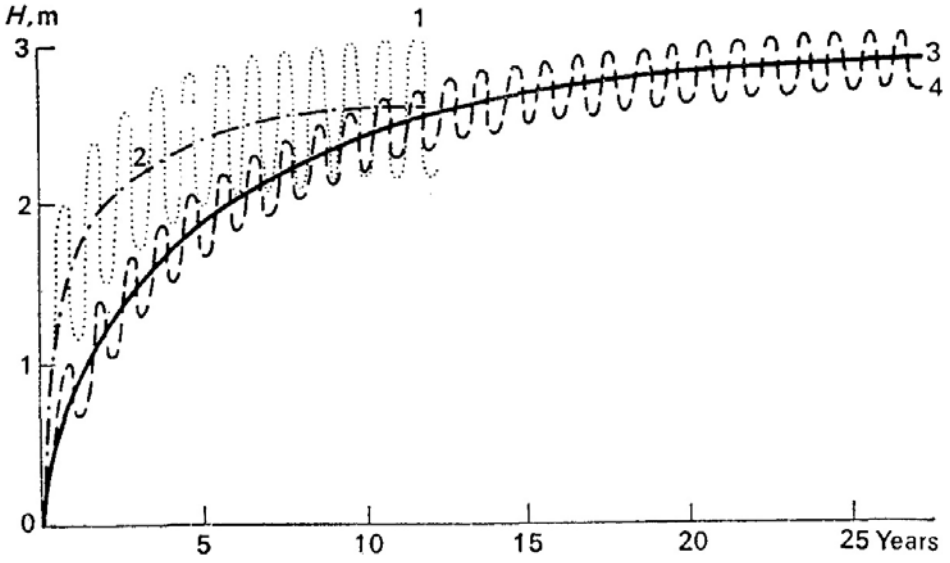

Figure 29. Forming equilibrium ice thickness. The dotted and dashed lines shows the monthly ice thickness (1 & 4) and the dot/dash and solid lines show the mean yearly thickness (2 & 3) near Wrangel Island (1 & 2), and Franz Josef Land (3 & 4). (From Doronin and Kheisin, 1977.)

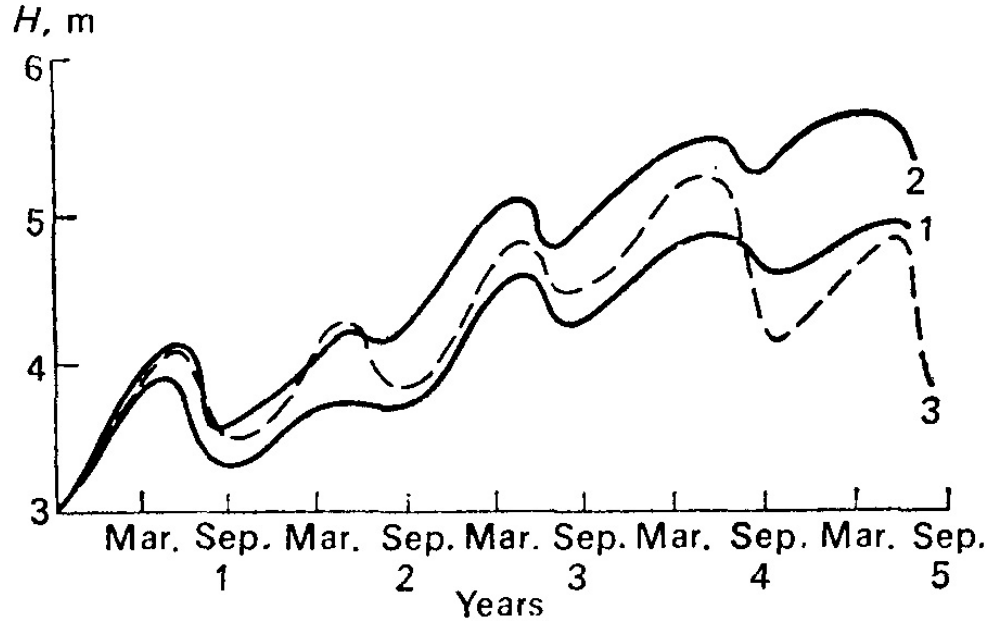

Figure 30. Change in ice thickness along a drift trajectory. Line 1 shows the ice thickness for a trajectory with snow and an ocean heat flux 0.6 kJ/(cm^2 month); line 2 shows the ice thickness with snow and an ocean heat flux of 0.0 kJ/(cm^2 month); and line 3 shows the ice thickness without snow and an ocean heat flux 0.6 kJ/(cm^2 month). [From Doronin and Kheisin, (1977).]

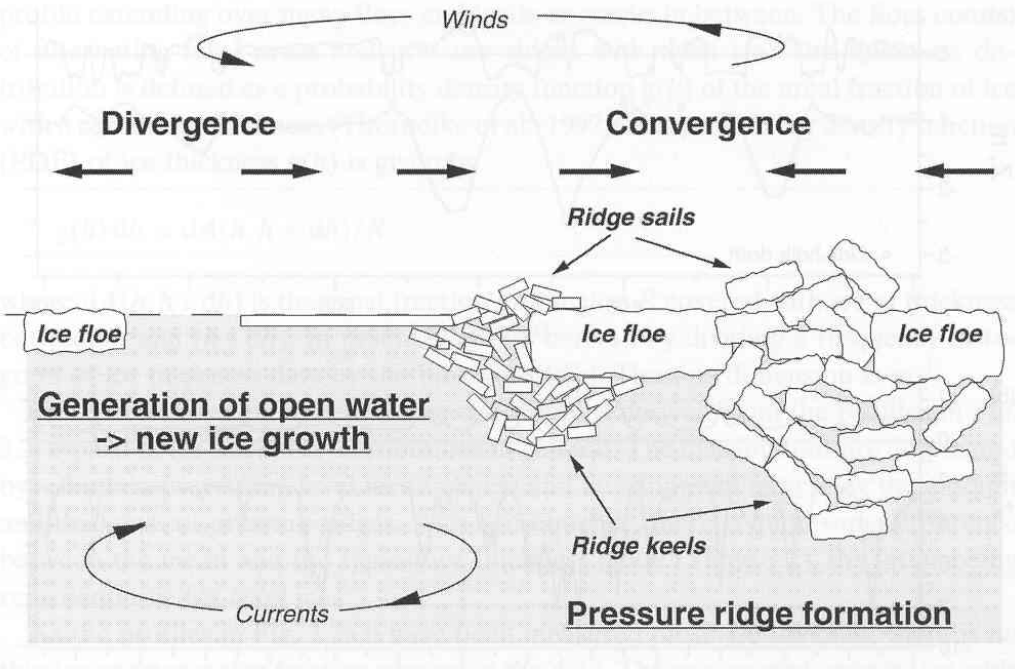

Figure 31. Illustration showing the production of open water and the ridging of sea ice driven dynamically by the winds. [From C. Haas (2003).]

growth of sea ice may be affected by more severe climatic conditions as it drifts on the Arctic Ocean, and by snow cover, which may hinder the melting of sea ice during summer. Doronin and Kheisin (1977) estimate that sea ice may grow to 4.8 m thickness after one circuit of the Beaufort Gyre (Fig. 30)[♦], however, sea ice may require a number of circuits of the gyre to attain its full thermodynamic equilibrium thickness, which may take decades. The thickness of sea ice may also be increased over time by wind stress on the sea ice (Fig. 31). The winds may create areas of open water and sea ice ridges by blowing sea ice away from or towards the coast, and by the Ekman drift of sea ice to the

[♦] Figure 17, for example, shows the drift of NP-22 from 1973 – 1982, which completed one circuit in about 6 years.

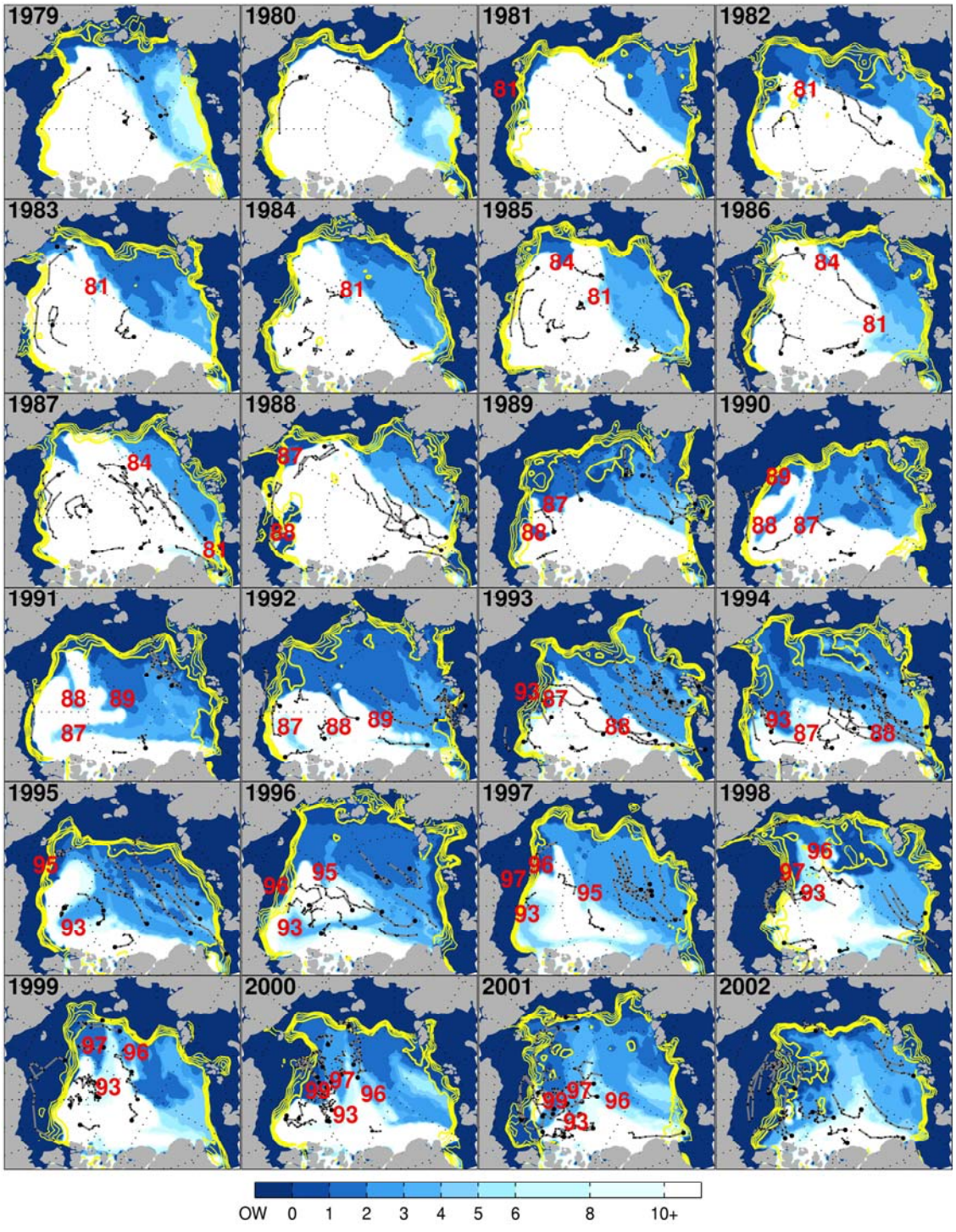

Figure 32. Estimated age of sea ice in September from 1979 to 2002 based on simulation. Color scale and contours are the same as in Fig. 17. The red numbers indicate the year that different patches of younger ice formed in the Beaufort and Chukchi seas.

right of the wind. Initially these processes "conserve" the volume of sea ice, but over time, they serve to increase the areal average thickness of sea ice because new ice quickly grows in areas of open water during winter.

Figure 32 shows the year-to-year evolution of the age of sea ice on the Arctic Ocean from 1979 to 2002 as inferred from the model described in Section 2d.[*] In order to validate the age of sea ice model as a proxy for sea ice thickness, we compared these results with estimates of the sea ice thickness climatology from satellite altimeter data (Laxon et al. 2003), and observations of sea ice thickness (draft) from submarines for each year from 1991 to 1997.

[*] An animation of this data is available on http://www.atmos.washington.edu/~ignatius/Dissertation/.

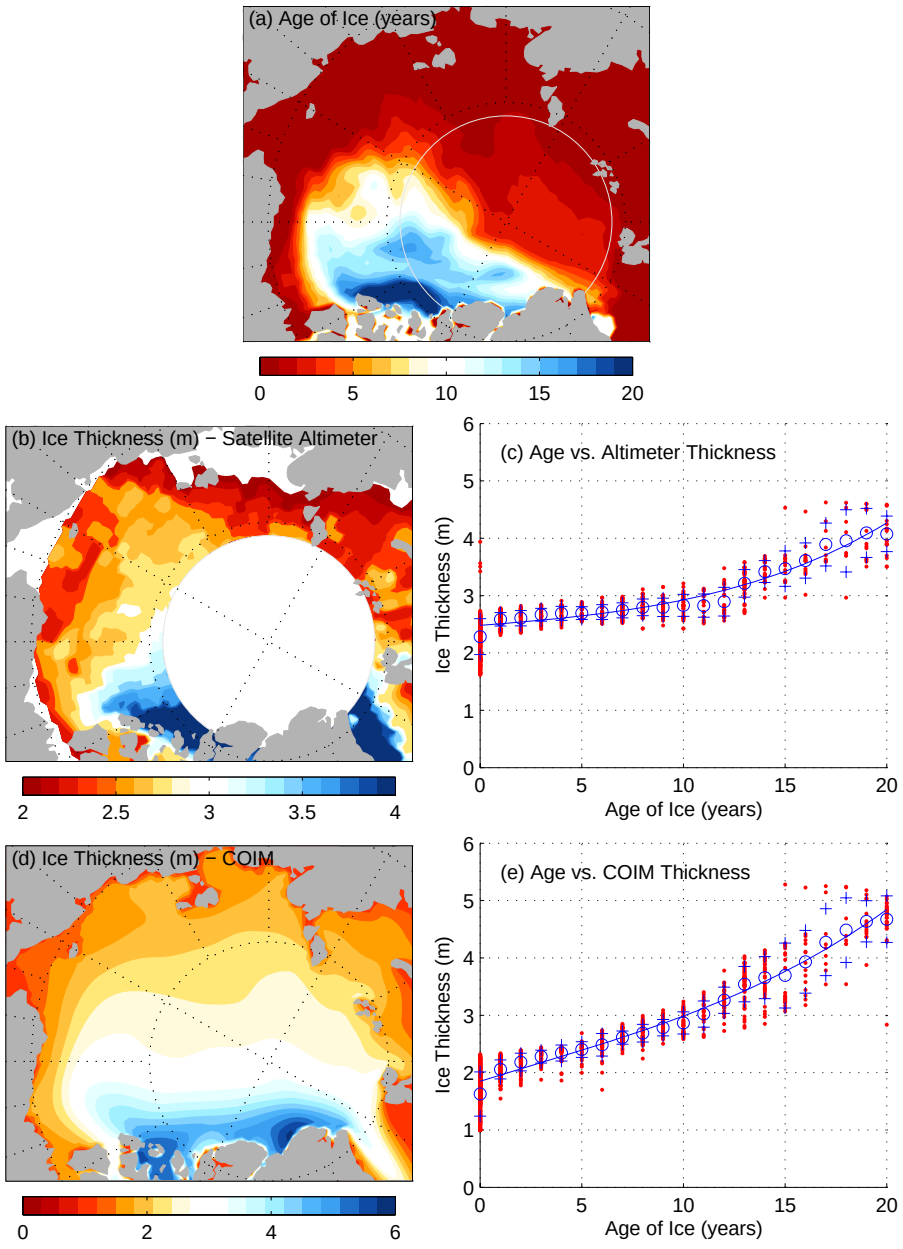

Figure 33. Comparison of ice age with ice thickness estimates from satellite altimeter data and coupled ocean-ice model (COIM) during winter (ONDJFM) for 1993–2001; The white circles over the north pole mark the area that is not covered by the satellite data. (c) scatter plot of age vs. altimeter ice thickness for coinciding grid points from 120E -60W (the area left of the north pole). The open circles show the mean thickness for each age, the + sign marks +/- 1 SD, and the line shows the cubic polynomial fit to the mean thickness estimates for each age; (e) same as (c) except for COIM ice thickness estimates.

a. Comparison of Estimates of Sea Ice Age and Thickness

The estimated thickness of sea ice from satellite altimeter data during winter (ONDJFM) 1993–2001 (Laxon et al. 2003) (Fig. 33a) is compared with the estimated age of sea ice for the same period in Fig. 33b. The patterns are generally similar, with younger sea ice where the modeled sea ice is thinner and vice versa. Figure 33c shows the age and thickness of sea ice at coinciding points from 120°E–90°W, with a cubic polynomial fit through the mean thickness for each age. The RMS difference between the cubic polynomial for all points is 0.3 m. Figure 34a shows the expected thickness of sea ice based on the cubic polynomial fit between the age and thickness estimates shown in Fig. 33c. The differences between the estimated sea ice thickness from the satellite altimeter and the expected sea ice thickness based on the age of sea ice is shown in Fig. 34c. Over most of the Arctic Ocean, the differences are less than 0.5 m, except in Fram Strait (area "A" in Fig. 34b).

The expected thickness based on the age of the sea ice was also compared with the estimated thickness of sea ice from a coupled ocean–ice model (COIM; Zhang and Rothrock, 2003) for the same period as the satellite altimeter climatology for sea ice thickness. The sea ice thickness estimates based on age and the COIM are qualitatively similar. However, the area of thicker ice simulated by the COIM extends farther eastward along the Canadian Archipelago and north of Greenland. The difference map between the estimated sea ice thickness from the satellite altimeter and the COIM show large areas in which the estimates based on the satellite altimeter are thicker than

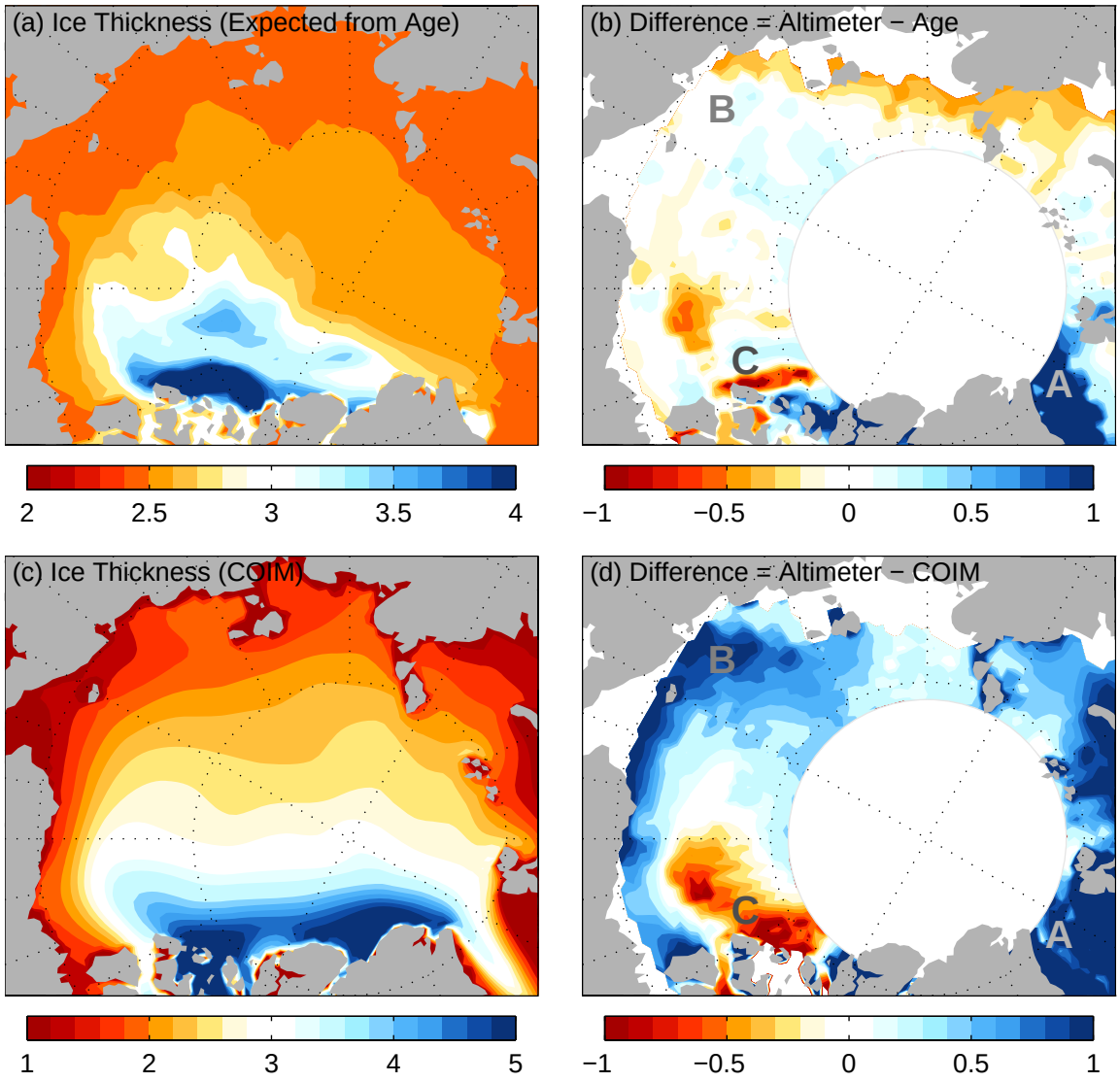

Figure 34. Expected ice thickness based on the cubic polynomial fit (Fig. 5c) during winter (ONDJFM) for 1993–2001 (a), and the difference between sea ice thickness estimates from the satellite altimeters (see Fig. 5a) and those based on age (b). For comparison, also shown are the mean ice thickness estimated from a coupled ocean-ice model (COIM) for the same period (c), and the difference between the estimates of ice thickness from the satellite altimeter data and COIM (d). The letters (A, B, C) mark areas discussed in the text. Note that the scale is different for the age and COIM ice thickness climatologies.

simulated in the COIM (areas ‘A’ and “B” in Fig. 34d). The area marked by a “B” in Fig. 34d is also an area of younger sea ice as shown in Fig. 34a.

Figure 33e shows the change in sea ice thickness with age estimated from our simple age model and the COIM. New sea ice formed during winter quickly grows to 1.5m thickness, and the ice continues to grow from 2.0m to 4.5m during the next 20 years. In comparison, the sea ice thickness estimated from the satellite climatology (Fig. 33c grows to 2.3m during the first winter, and then grows more slowly to 4.0m during the next 20 years.

The estimated thickness of young sea ice as inferred from the satellite altimeter data is higher than expected based on the thermodynamic growth of sea ice less (Fig. 29), and as estimated by the COIM (Fig. 33e). Although this rapid thickening may be due to the ridging and rafting of sea ice, it is also possible that there may be a high bias in the estimates of sea ice thickness from the satellite altimeters in areas where new ice forms because the procedures of Laxon et al. (2003) exclude estimates of sea ice thickness less than 1 meter from the climatology (since these estimates have a low signal-to-noise ratio). This bias may also explain why the sea ice that is thicker than expected based on age and the COIM in Fram Strait, which is an area of high divergence that may have more patches of younger, thinner ice (area “A” in Figs. 34b and 34d). The difference map between the satellite altimeter estimates and the COIM also shows an area of sea ice where the COIM simulations may overestimate the thickness of sea ice in the Canadian Basin (area “C” in Fig. 34d, and Fig. 33e). This difference may have some implications for the COIM’s ability to simulate the extent of

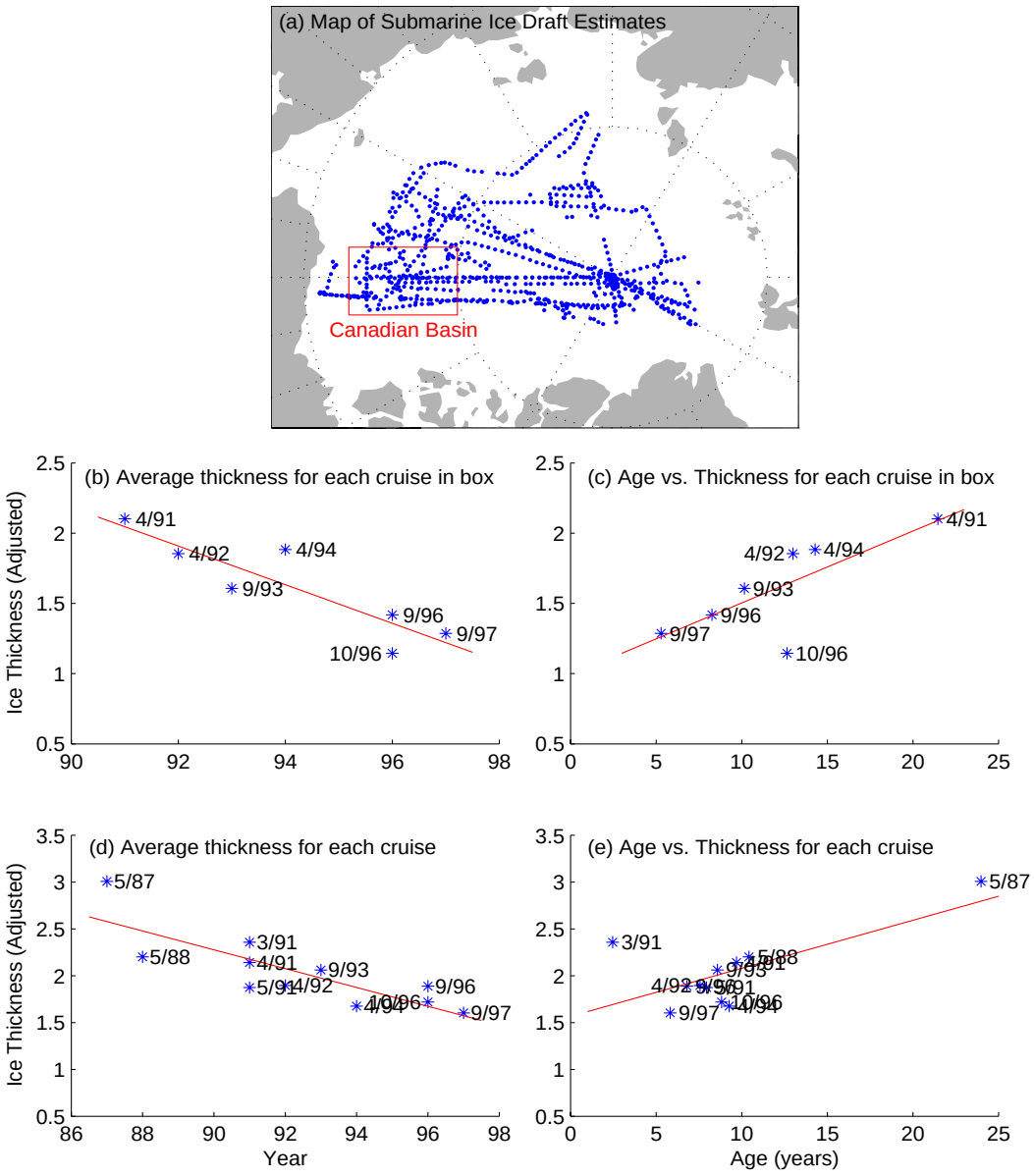

Figure 35. (a) Map showing the locations of sea ice thickness (draft) measurements from upward looking sonar on submarines from 1987 to 1997. Measurements of sea ice draft were converted to thickness by multiplying by 1.12. The red box marks the area where Yu et al. (2004) estimates ice thickness distributions for the Canadian Basin; (b) the mean thickness of sea ice along submarine tracks during different cruises in the box; each point is labeled with the month and year of the cruise; (c) the mean age of sea ice plotted against the mean thickness along each track in the box. The April estimates were adjusted downward by 1.1 m, to account for the annual cycle of sea ice thickness, and match the September estimates; (d) shows the average thickness of all points for each cruise; and (e) shows the mean age plotted against thickness for all points of each cruise.

summer sea ice along the Alaskan coast. In contrast, the estimates of thickness based on age are closer to the observations, and the differences appear in bands of alternating high and low differences, which may imply that the age model captures the "gross" spatial features of the sea ice thickness climatology, but exhibits some small errors in the location of these features (area "C" in Fig. 34b).

Figure 35a shows the locations of sea ice thickness draft measurements from upward looking sonars on submarine cruises from 1986 to1998. The red box marks the Canadian Basin, which is closest to the area where the largest decreases in sea ice extent along the Alaskan coast were observed, and where Yu et al. (2004) report the changes sea ice thickness distributions for the periods 1958–1976 and 1993–1997. For these periods, Yu et al. (2004) estimate a decrease in the mean thickness from 3.1 m to 1.81 m, a difference of 1.3 m. They show that most of this decrease was due to a 42% decrease in the areal coverage of sea ice thicker than 3 m. Comparisons of our age model to the earlier data (1958–1976) are difficult because our model is initialized in September 1954 with the assumption that sea ice with in the sea ice extent limit was just one year old. For the later period it is possible to estimate the thickness and age of sea ice in the box for each year from 1991 to 1997.

Figure 35b shows the mean sea ice thickness, and the month and year of each submarine cruise. To account for the annual cycle of sea ice thickness and make the April estimates comparable to those taken in September, the April estimates were

adjusted by lowering them 1.1 m[†]. The mean sea ice thickness in the Canadian Basin decreased from 2.0 m in 1991 to 1.2 m in 1997. Figure 35c shows the mean sea ice thickness and age along each cruise track. Apart from the one outlying estimate in October 1996, the estimates of age and sea ice thickness agree well (R = 0.8 for all points; R = 0.96 if the October 1996 estimate is ignored).

Figures 36d and 36e show the mean thickness for each cruise during different years, and the mean thickness and age of sea ice along the entire track of each cruise, respectively. In comparison to Figs. 36b and 36c, these figures show a similar decline in the thickness of sea ice over time and an increase in the thickness of sea ice with age. However, the relationship between the age and thickness of sea ice over the Arctic Ocean as a whole (Fig. 36e) is not as clear as this relationship is for specified areas like the Canadian Basin (Fig. 36c). Part of this ambiguity may be due to slight displacement errors in the age model. For example, the cruise during March 1991 sampled along an area where these was a steep gradient in the estimated age of sea ice. A slight shift in the location of this gradient would have greatly increased the estimated age of sea ice along this track, and improved the fit of this point with the other data. However, the coverage of the submarine data is limited in space and time so this ambiguity may also be due to differences in the areas sampled by the submarines from one year to the next. Thus, the relationship between the changes in sea ice thickness with age is clearer for localized areas like the Canadian Basin (Fig. 36c).

[†] The annual cycle of sea ice thickness for the Canadian Basin was estimated from the COIM for the period 1991 – 1997.

b. Interdecadal Variations in the Age of Sea ice

The age of sea ice model indicates that during the past 15 years the area of old ice is much smaller than it was prior to 1989 and that during recent years the sea ice has been especially thin north of Alaska. These conditions may have evolved on an interannual time scale, during relatively low AO-index conditions, as were prevalent during the 1980's; ice recirculates in the large Beaufort Gyre for over 10 years (also see Fig. 17), and younger sea ice formed during summer in the Beaufort and Chukchi seas are advected away from the Alaskan coast into the Eurasian Arctic, and drift out of the Arctic Ocean through Fram Strait. For example, sea ice formed in the Chukchi Sea in 1981 drifts with the Beaufort Gyre into the Eurasian Arctic Ocean and leaves the Arctic Ocean through Fram Strait in 1987. During this period ~80% of the area of the Arctic is covered by thick, multi-year ice.

With the transition to extreme high-index AO conditions in 1989, the area of the Arctic Ocean covered by old sea ice decreases precipitously (Fig. 32). These changes are driven by AO wind anomalies, which reduce the size of the Beaufort Gyre (e.g. see Fig. 23), thus decreasing the drift of ice into the Eurasian Arctic, and increasing the advection of multi-year ice away from the Eurasian coast towards the Canadian Arctic and out through Fram Strait. By the end of summer 1990 in the simulation, the fraction of the Arctic Ocean covered by ice older than three years drops from ~80% to 30%. The spatial changes in the age of ice as inferred from the model agree with the observed decrease in ice thickness (Rothrock, et al. 1999), and the observed and modeled

decrease in the fraction of ridges on the Arctic Ocean (Yu, et al. 2004; and Makshtas, et al. 2003).

With the reduction of the area covered by the Beaufort Gyre, less old ice from the central Arctic is exported into the seasonal ice zone along the Alaskan coast, and the age of sea ice recirculating back into the seasonal ice zone from ice drops from over 10 years (Fig. 17 and Fig 32 prior to 1989) to 3–4 years (Fig. 32, after 1991). For example, in 1997 (Fig. 32) the model shows recirculation of young ice back into the seasonal ice zone. The two intrusions of young ice along the edge of the old ice area in the central Arctic in September 1997 are comprised of new ice formed in areas of open water along the Alaskan coast after the summers of 1995 and 1996. The large area of young ice recirculating back into the seasonal ice zone along the Alaskan coast in 1997 was produced in the large area of open water in the Chukchi Sea during the autumn of 1993. The large deviations between the summer sea ice concentration EC time series and the summer AO index (Fig. 20) begin around 1997 when younger (thinner) ice is advected into the Beaufort and Chukchi seas.

In the simulation low-index AO conditions during summers of 1997, 1998, and 1999 force the further depletion of the reservoir of old ice remaining in the Beaufort Gyre, and the retreat of sea ice extent is enhanced by the advection of younger (thinner) ice into the area. The moderately high AO conditions averaged over these calendar years has the effect of recirculating younger and younger sea ice back to the Alaskan coast, thereby compounding the decreases in sea ice extent each summer, producing the ice conditions observed today (Fig. 17 and 32). During the 2002 and 2003 summers

this anomalously young, thin ice was advected into Alaskan coastal waters (Fig. 32) where extensive melting was, in fact, observed, even though temperatures were locally colder than normal (Serreze et al., 2003).

In contrast to the above hypothesis, Serreze et al. (2003) argue that the sea ice extent minimum of 2002 resulted from the increased advection of heat onto the Arctic Ocean during spring, and persistent low pressure and high temperatures during summer. These conditions are consistent with the prevalence of high AO conditions during summer of 2002. While it is plausible that these mechanisms may have contributed to reducing the concentrations of sea ice over the Arctic Ocean, the hypothesis offered here may provide a better explanation for the 2002 and 2003 minima over the coastal areas of the Beaufort and Chukchi seas. Specifically, the observed negative anomalies in sea level pressure over the Arctic Ocean may have increased the divergence of sea ice, giving rise to an increased area of open water over the central Arctic Ocean, but this divergence would have acted to push ice towards the coastal areas, and indeed this is observed in the drift of buoys during the summer of 2002. And although the temperatures were slightly above normal over the central Arctic Ocean, as noted earlier, the temperatures were below normal over the Beaufort and Chukchi seas where the largest decreases in sea ice extent were observed (See Fig. 3 of Serreze, et al. 2003). However, if the recent minima are attributable to the advection of younger, thinner ice into the coastal melt zones of the Arctic Ocean as hypothesized, then the anomalies produced by the mechanisms that Serreze, et al. (2003) proposed, which would have increased the production of younger, thinner ice over the central Arctic Ocean, would

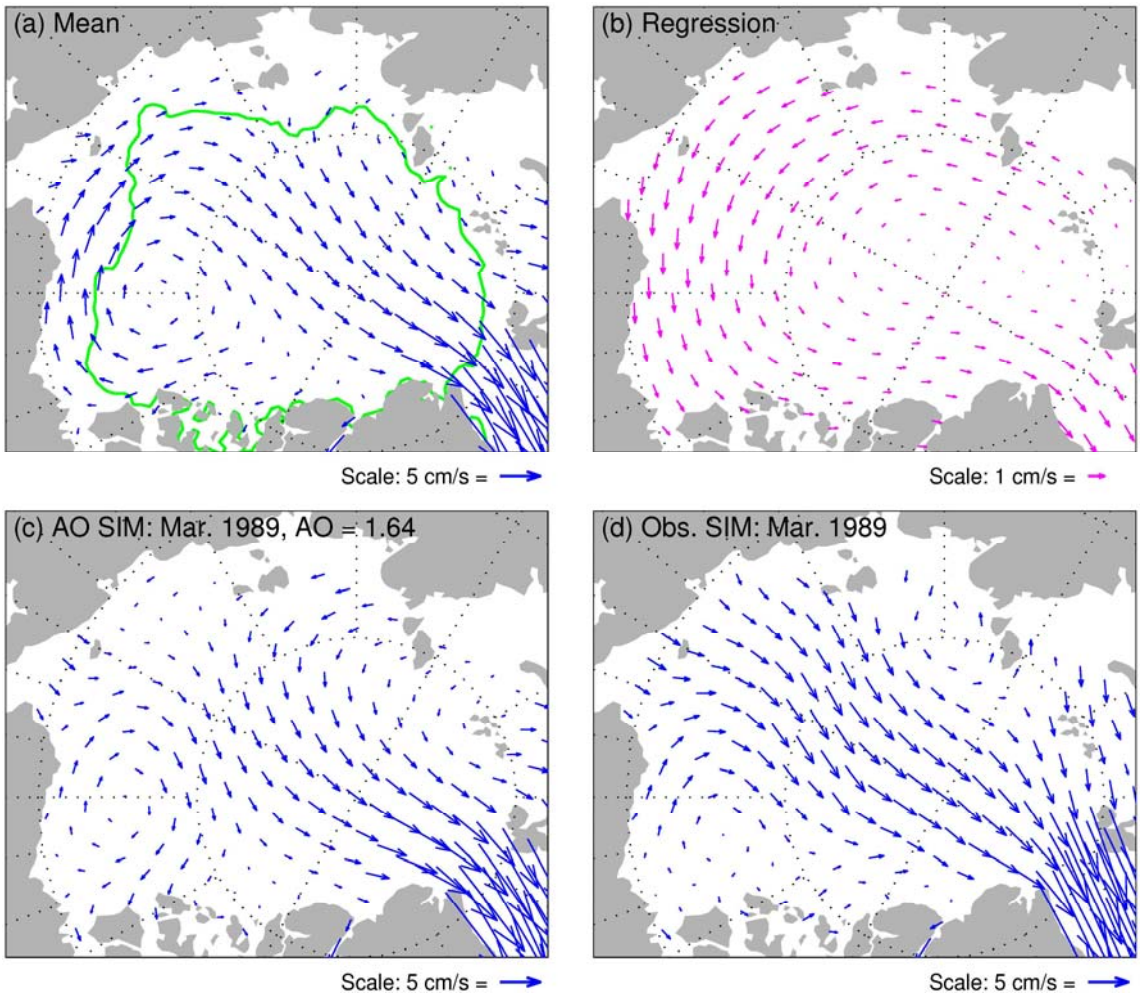

Figure 36. Sea ice motion related to the AO: (a) mean field of sea ice motion and sea ice concentration, (b) regression of the monthly sea ice motion on the AO index, (c) shows the sea ice motion related to the AO (AO = 1.51), and (d) observed sea ice motion field for March 1989. (c) captures the weakening of the Beaufort Gyre and the advection of ice away from the East Siberian Sea, however, (d) shows much stronger transpolar flow related to the second EOF of sea ice motion (PC2 = 1.1, see Fig. 21).

enhance the anomalies in sea ice extent in future years as this younger, thinner ice drifts into the coastal melt zones of the Arctic Ocean. For example, the sea ice extent anomaly off the Alaskan coast in 1997 may have been much stronger than expected given the atmospheric conditions (Fig. 20) because younger (thinner) sea ice produced in the Beaufort and Chukchi seas in 1993 had recirculated back into this area to enhance the decrease in sea ice extent.

c. Simulations Based on Simplified Forcing

To determine the conditions required to produce the estimated decrease in the age of sea ice throughout the Arctic Ocean and the contribution of the AO to the changes in the age of sea ice and sea ice extent in the Beaufort and Chukchi seas, a series of additional simulations were performed in which the sea ice extent was prescribed as either the observed, or the climatological mean September sea ice extent (Fig. 37a), and sea ice motion used to force the simulations was prescribed as either the observed, climatological mean (Fig.. 37a), or high and low AO composites. In the following discussion reference to the "complete model run" (Fig. 32) means the model run based on the total observed sea ice motion and sea ice extent.

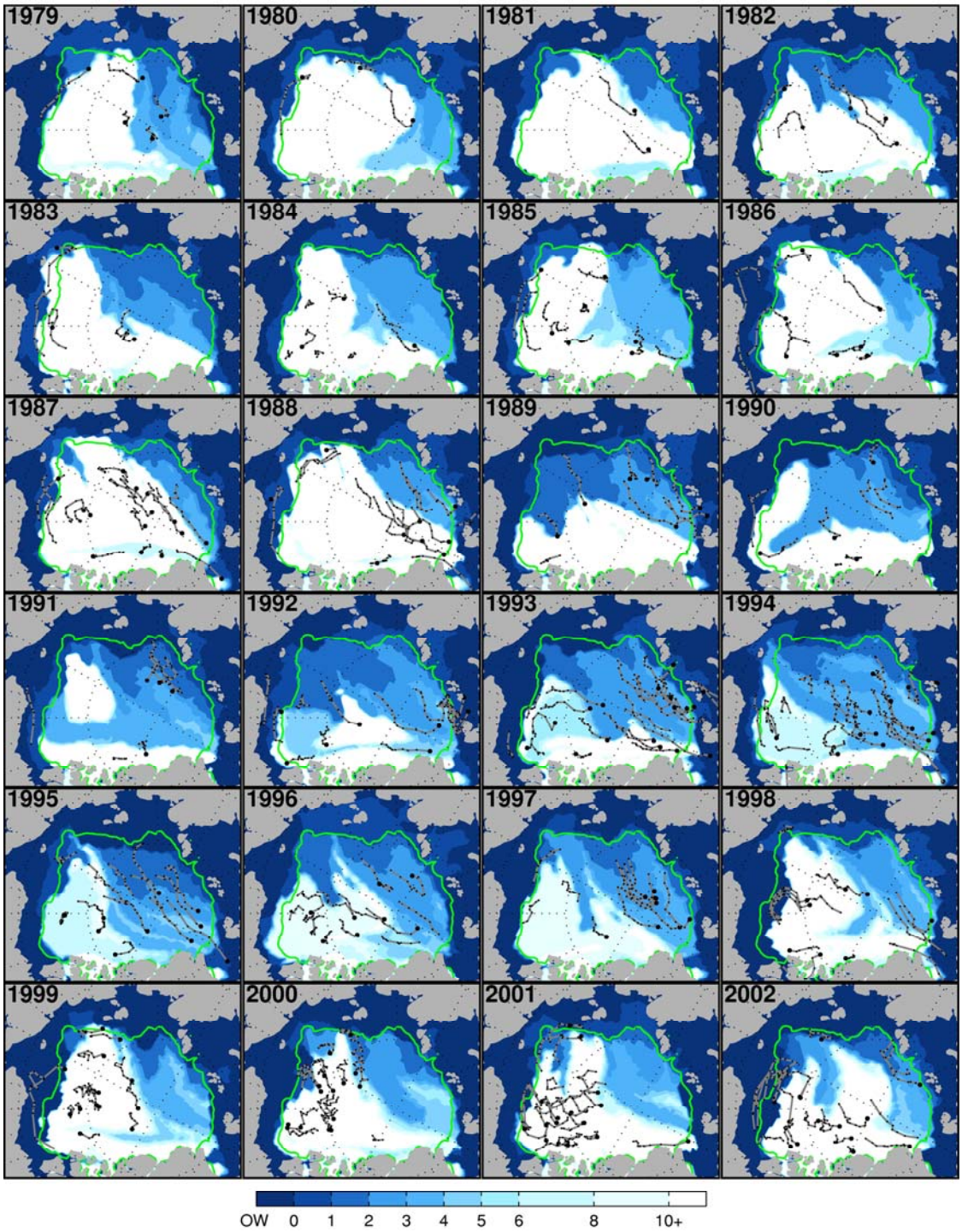

Figure 37. Age of sea ice from 1979–2002 based on simulations using the mean September sea ice extent, and observed sea ice motion. Contour shows climatological mean 90% sea ice concentration isoline.

The first experiment explores the role of sea ice motion in determining the age of the sea ice. The model was run using the climatological mean sea ice extent (Fig. 36a)[♦] and the observed monthly sea ice motion. The results for this simulation are shown in Fig. 37. This simulation exhibits a large area of old sea ice in the early 1980's, but this area is not as large as the area of old sea ice estimated in the complete model run. This smaller areal coverage is due to the fact that the extent of sea ice was greater than the mean in the early 1980's. Thus this simulation overestimates the decrease in the age of sea ice during this period, leading to an underestimate of the area of old sea ice. This simulation captures the precipitous decline in the age of sea ice with the step to high-AO conditions in 1989, and the recirculation of younger sea ice back to the Alaskan coast during the extreme high-AO period of the early 1990's. However, it doesn't capture the continued decline in the average age of sea ice in the late 1990's shown in the complete model run when the AO index returns to near normal conditions (Fig. 11). In fact, this simulation shows some tendency toward a recovery of the old sea ice after 1995 when the AO index returned to near normal.

[♦] The climatological mean sea ice extent is defined as the 90% sea ice concentration isoline of the climatological mean field of sea ice concentration from 1955 – 2002 (green line in Figs. 27 and 28).

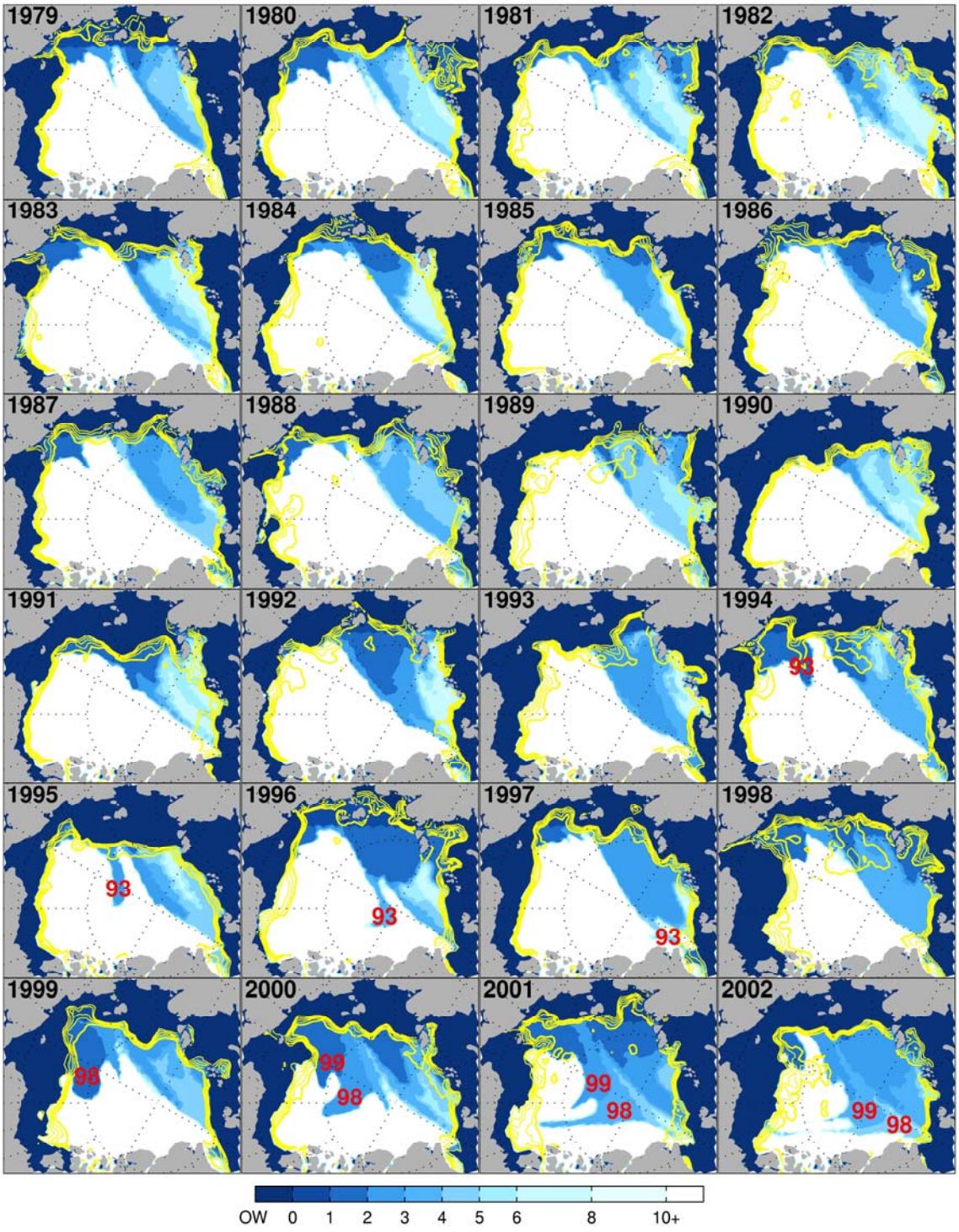

Figure 38. Age of sea ice from 1979–2002 based on simulations using the observed September sea ice extent, and climatological mean sea ice motion. Contour shows climatological mean 90% sea ice concentration isoline. The red numbers indicate the year that different patches of younger ice formed in the Beaufort and Chukchi seas.

The second experiment explores the role of the variations in sea ice extent in producing the estimated age of sea ice in the complete model run. The model was forced with the observed September (year-to-year) sea ice extent and the climatological mean sea ice motion (Fig. 36a). The results for this simulation are shown in Fig. 38. In this simulation the dramatic decrease in the age of sea ice from 1989–1990 observed in the complete model run (Fig. 32) does not occur, and younger sea ice formed along the Alaskan coast during the 1990's is not recirculated back to the Alaskan coast (Fig. 32). However, there is a decrease in the estimated age of sea ice in the 1990's in the central Arctic as new ice formed in the large areas of open water along the Eurasian and Alaskan coasts during fall are swept away from the coast into the Transpolar Drift Stream towards Fram Strait. The results of these first two experiments imply that the variations in sea ice motion and sea ice extent are both necessary to reproduce the estimated age of sea ice in the complete model run.

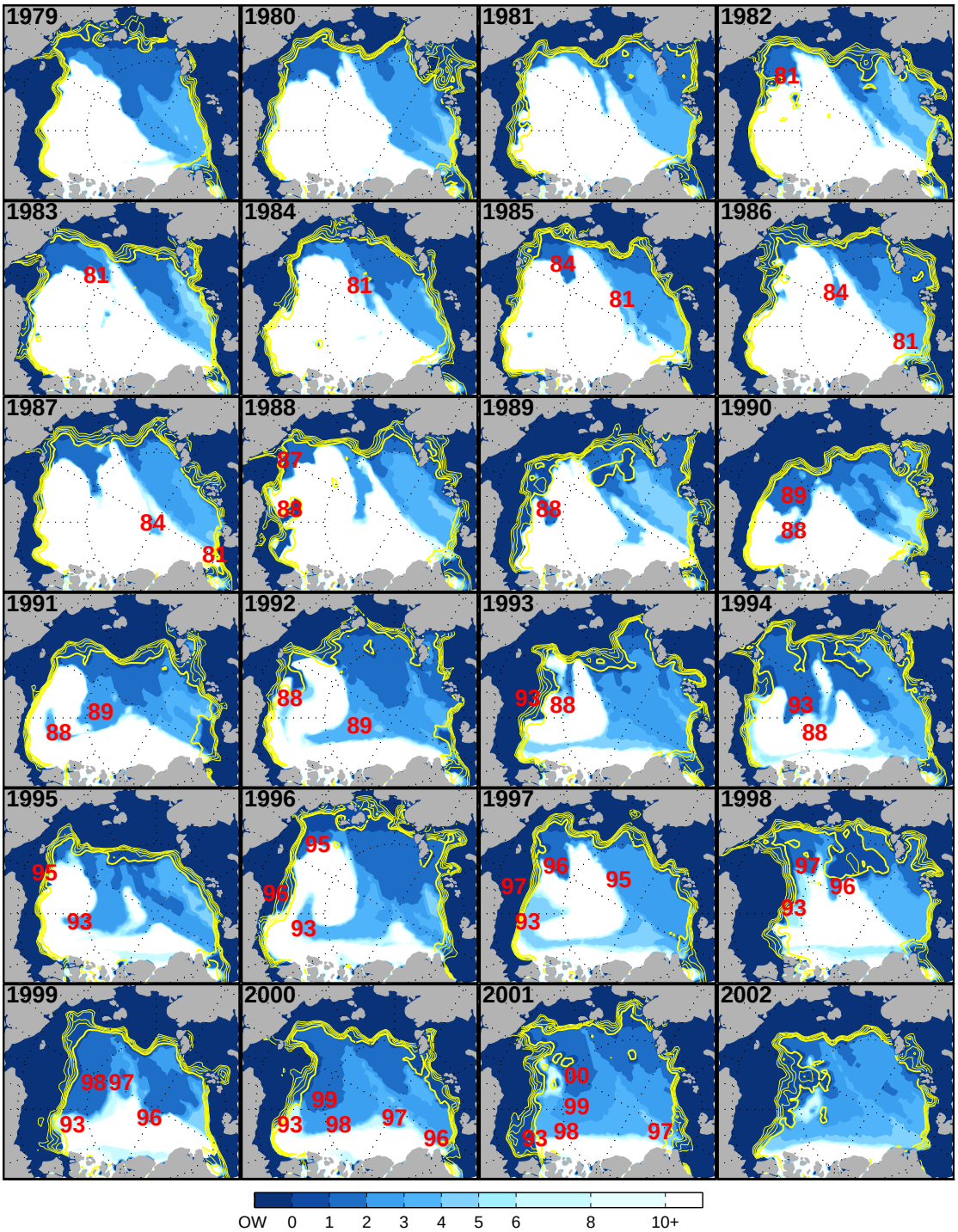

Figure 39. Modeled age of sea ice from 1979–2002 based on simulations using the observed September sea ice extent for each year, and sea ice motion related to the Arctic Oscillation. Color shades and contours are the same as in Fig. 17. The red numbers indicate the year that different patches of younger ice formed in the Beaufort and Chukchi seas.

The third experiment explores the role of variations in sea ice motion related to the AO in producing the estimated age of sea ice in the complete model run. The model was forced by only the part of the sea ice motion related to the AO and the observed September sea ice extent for each year. In these experiments the sea ice motion related to the AO for each month is estimated by taking the regression coefficient of sea ice motion on the AO index at each grid-point, multiplying it by the AO index for each month, and adding the product to the mean field of sea ice motion. For example, the estimated field of sea ice motion related to the AO for August 1989 is shown in Fig. 36c. The results for this simulation are shown in Fig. 39. This simulation captures all of the critical events observed in the complete model run such as the decrease in the age of ice during 1989 and 1990, the reduced circulation of the Beaufort Gyre, the recirculation of younger sea ice produced along the coast in 1993 back to the coast in 1997, and the dramatic decrease in the age of ice in the gyre. Hence we conclude that the time varying AO captures the essence of the wind forcing of the sea ice motion field that leads to the decline of Arctic sea ice.

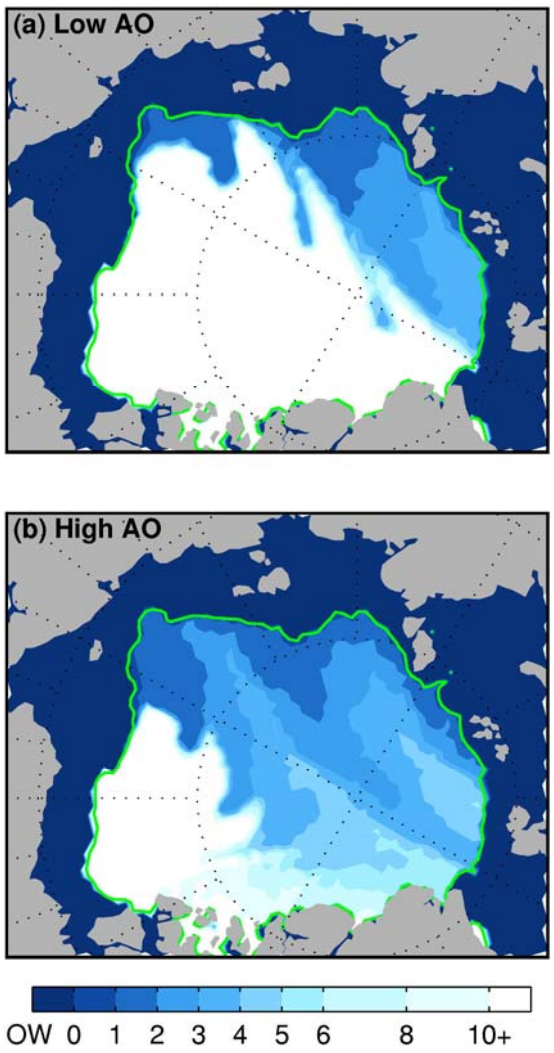

Figure 40. (a) Modeled estimate of the age of ice for persistent low AO conditions (AO = -1.0), and (b) persistent high AO conditions (AO = 1.0). Contour shows climatological mean 90% sea ice concentration isoline.

The fourth experiment explores the differences in the average age of sea ice when the model is forced with persistent low and high AO sea ice motion. In the high-index simulations the AO index was set equal to +1, and in the low-index simulations the AO-index was set equal to –1. The sea ice extent was fixed at the climatological mean. Figure 40 shows the estimated age of sea ice from these simulations after integrating the model for 15 years (after 10 years the annual cycle in the age of sea ice repeats itself with little further year-to-year changes). In the low AO sea ice motion simulation (Fig. 40a) the Beaufort Gyre is large, and most of the sea ice on the Arctic Ocean is over 10 years old, but some young ice can be seen in the Transpolar Drift Stream. The notches of young ice into the area of old ice were produced in the Chukchi sea and are drifting towards Fram Strait. In the simulation forced with high AO sea ice motion, the Beaufort Gyre is reduced, and a larger area of young ice is seen in the Transpolar Drift Stream, but a pool of old ice remains trapped, recirculating in the Beaufort Gyre, which is not affected by "melt" because it is north of the climatological mean September sea ice edge (Fig 40b). This experiment shows that persistent high AO sea ice motion alone do not explain the changes in the age of sea ice estimated in the complete model run.

A fifth experiment explores the role of the variations in sea ice extent in producing the estimated age of sea ice in the complete model run. The model was forced with the observed September (year-to-year) ice extent and either persistently low or high AO sea ice motion. In the low AO sea ice motion simulation younger sea ice formed along the Alaskan coast was simply swept away towards Fram Strait (Fig. 41).

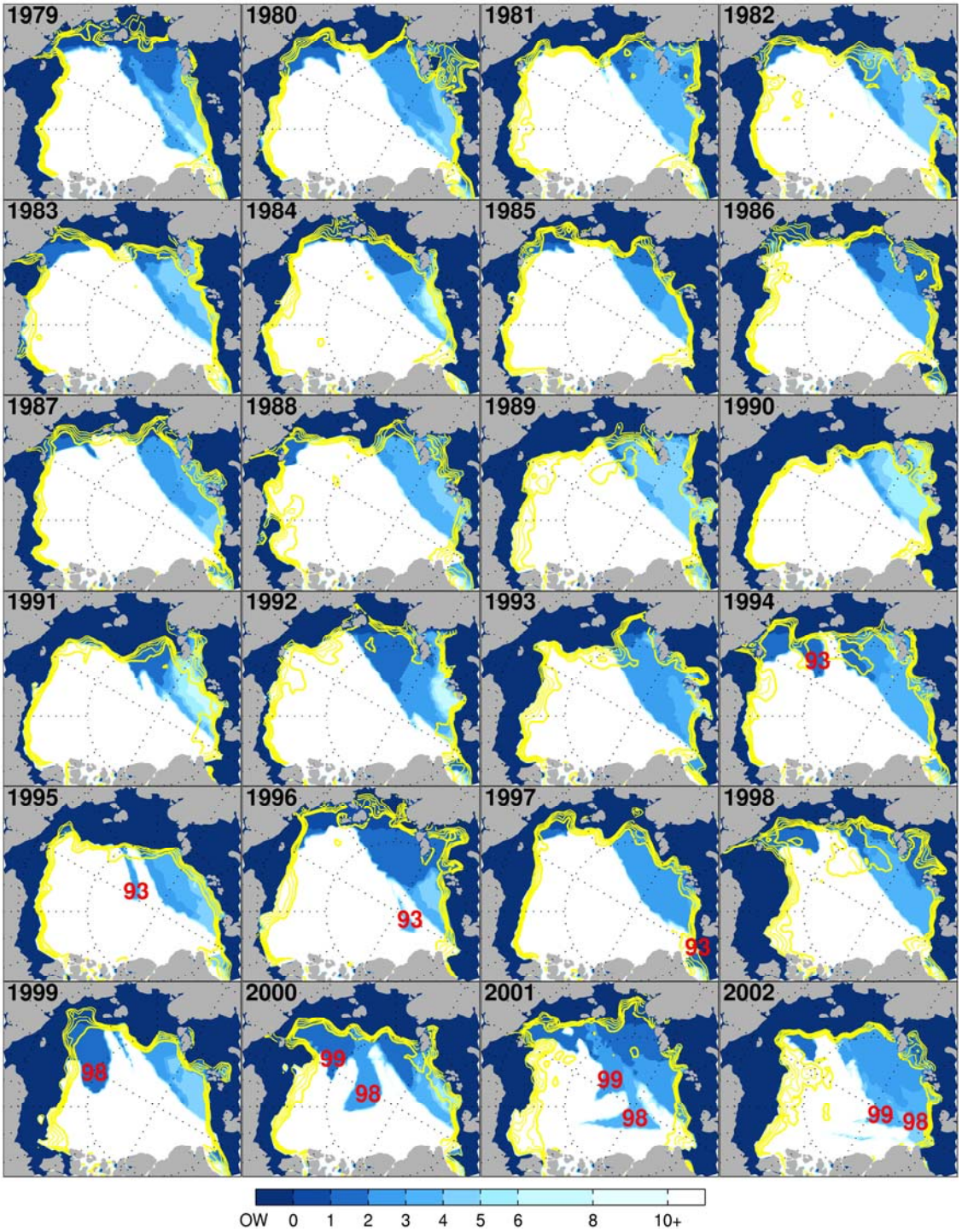

Figure 41. Age of sea ice from 1979 to 2002 based on simulations using the observed September sea ice extent for each year and low AO sea ice motion. Color shades and contours are the same as in Fig. 17. The red numbers indicate the year that different patches of younger ice formed in the Beaufort and Chukchi seas.

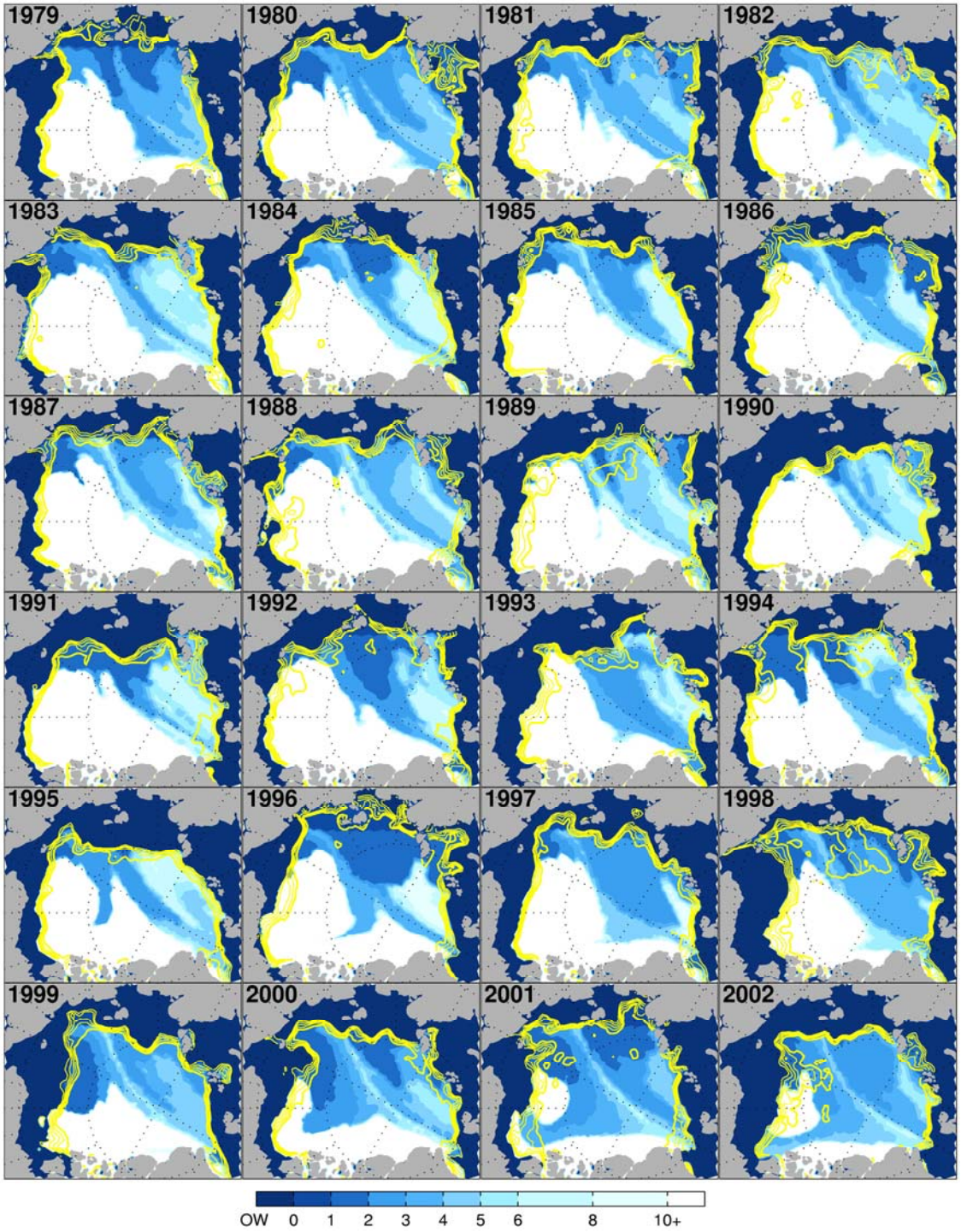

Figure 42. Age of sea ice from 1979 to 2002 based on simulations using the observed September sea ice extent for each year and high AO sea ice motion. Color shades and contours are the same as in Fig. 17.

In the simulation based the observed September sea ice extent and persistently high AO sea ice motion, younger sea ice formed along the coast was trapped within the Beaufort Gyre and the age of sea ice was much lower than estimated in the complete model run during the 1980's, but higher than the complete run in the late 1990's (Fig. 42). These differences can be explained by the fact that the AO index was lower during the 1980's than in the simulation, and during the 1990's the age of sea ice was older on average because the rapid decline in the age of sea ice, which was forced by a step to extreme high AO conditions observed in 1989 that was not simulated in this experiment.

These results imply that the necessary conditions for reproducing the observed decrease in the age of sea ice in the Beaufort and Chukchi seas are (1) a dramatic decrease in the age of sea ice driven by extremely high AO conditions of the early 1990's; (2) low sea ice extents during summer, which are related to low AO conditions that favor the advection of sea ice away from the Alaskan coast, thus the decrease in sea ice extent; and (3) high AO conditions averaged over the year, which result in the recirculation of younger (thinner) sea ice back to the Alaskan coast. All these conditions were satisfied when the model was forced by only the part of the sea ice motion related to the AO and the observed September sea ice extent for each year (Fig. 39). This simulation reproduced with a remarkably high degree of fidelity the decrease in the age of ice during 1989 and 1990, the reduced circulation of the Beaufort Gyre, the recirculation of younger sea ice produced along the coast in 1993 back to the coast in 1997, and the dramatic decrease in the age of ice in the gyre seen in the complete model run. Through this chain of events it hypothesized that the recent record low years in

Arctic sea ice extent may be interpreted as a delayed response to the 1989-1995 high-index AO event.

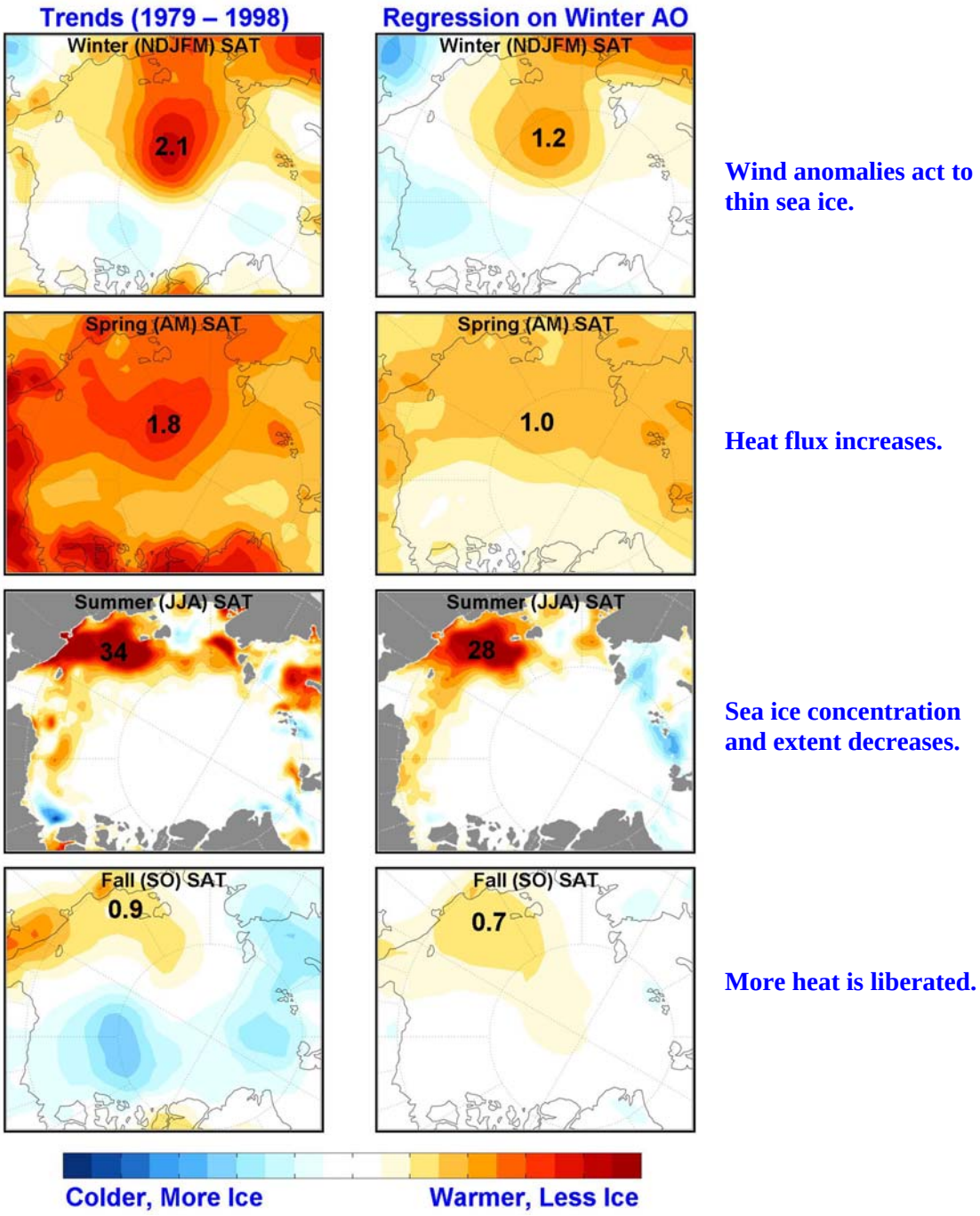

Figure 43. Seasonal memory of the prior winter AO. This figure shows the trends in surface air temperature and sea ice extent from 1979–1998 (left column), and the regression of these fields on the prior winter Arctic Oscillation index (right column). The winter map also shows the regression of sea ice motion on the Arctic Oscillation index. Adapted from Rigor et al. 2002.

5. Summary

This dissertation has explained the effect of the atmosphere on the variability of Arctic sea ice, and has investigated whether changes in the age of the sea ice might have contributed to the recent minima that have been observed in summer sea ice extent.

The AO affects sea ice on many different times scales. On seasonal time scales, increased advection of ice away from the East Siberian coast during wintertime high-index conditions of the AO enhances the production of new, thin ice in the flaw leads of the East Siberian and Laptev seas. The cyclonic sea ice motion anomalies that occur in association with the high-index polarity of the AO also enhance the production of new, thin ice during winter by increasing Ekman divergence over the eastern Arctic. Both these processes contribute to the thinning of sea ice, increasing the flux of heat into the atmosphere and warming surface air temperature. Changes in sea ice motion have evidently contributed to the observed decreases in ice area and extent, and the thinning of sea ice over the Arctic since the 1980's. Naively, one might have expected the warming trends in surface air temperature to cause the thinning of sea ice, but the results presented in Rigor et al. (2002) imply the inverse causality; i.e., the thinning ice has warmed surface air temperature by increasing the heat flux from the ocean. This inference is supported by estimates of the distribution of horizontal temperature advection presented in Section 3 of this dissertation.

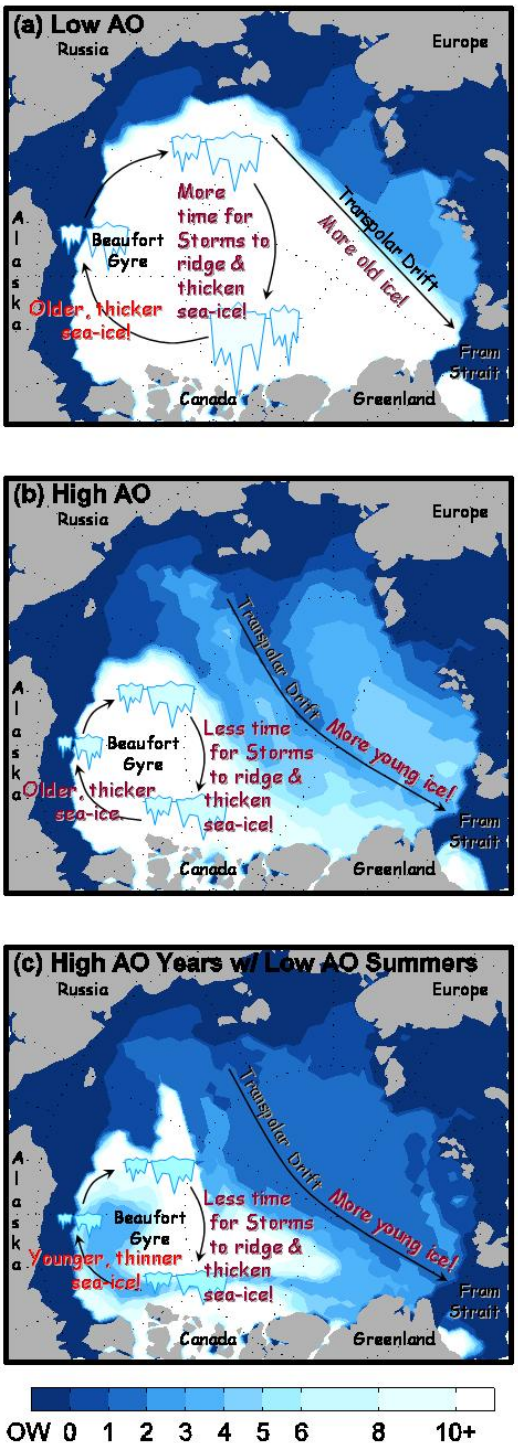

Figure 44. (a) Modeled estimate of the age of ice for persistent low AO conditions (AO = – 1.0), (b) persistent high AO conditions (AO = 1.0), and (c) for 1997 after years of moderate to high AO conditions with some low AO summers. (c) shows the return to the Alaskan coast of younger sea ice produced during the summer of 1993.

Sea ice provides memory for the arctic climate system so that changes in sea ice motion driven by the wintertime AO can be felt during the ensuing seasons (Fig. 43); i.e., the AO drives dynamic thinning of the sea ice during winter, allowing more heat to be released from the ocean through the thinner ice during spring, and resulting in lower sea ice concentration during summer and more heat liberation by the freezing of the ice in autumn. These delayed effects imply that a change in the length of the sea ice melt season may be dynamically driven by the prior winter AO because increased heat flux during spring may accelerate the onset of melt, while the increases in open water during summer may increase the amount of insolation absorbed by the ocean thus delaying the onset of freeze in the autumn.

During summer a low-index phase of the AO favors a decrease in ice concentrations in the Beaufort and Chukchi seas through an increase in the advection of ice away from the coast (Fig. 23) and increase in the advection warm air onto the ice (Fig. 24, west of Barrow).

On the interannual time scale, low index AO conditions during summer favor the advection of sea ice anomalies away from the Beaufort and Chukchi seas in the enlarged Beaufort Gyre (Fig. 44a), and during moderate to high AO conditions, the smaller Beaufort Gyre recirculates younger sea ice back to the coast 3–4 years later (Fig. 44b), greatly reducing the time that sea ice has to ridge and thicken before returning for another melt season along the Alaskan coast. And when these younger,

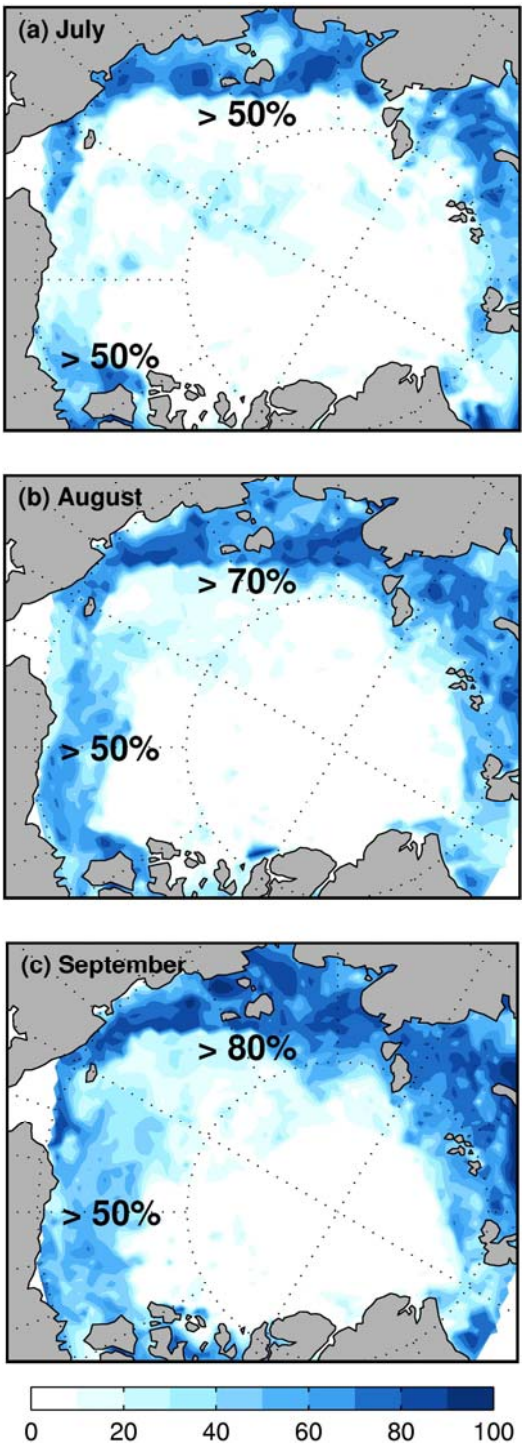

Figure 45. Fraction of the variance of July–September sea ice extent explained by the age of sea ice as inferred from the model.

thinner ice anomalies recirculate back to the Alaskan coast, they exacerbate the decreases in sea ice extent (Fig. 44c).

The transition to an Arctic Ocean dominated by "young" ice occurred abruptly in 1989–1990 when the AO index was over two standard deviations above normal much of the time. The reverse transition from present day conditions to a state like that which prevailed prior to 1989, with large areal coverage of old, thick ice, would obviously take much longer. When the model is forced with winds observed starting in 1950, the transition requires about 10 years; if winds starting in 1960 are used it requires 15 years or longer.

The winter AO index explains up to 50% of the variance in summer sea ice extent in the Eurasian sector, but the winter and summer AO indices combined explain only up to 15% of the variance along the Alaskan coast. In contrast, the age of sea ice explains over 50% of the year-to-year variability in summer sea ice extent (Fig. 45). If this interpretation is correct, low summer sea ice extents are likely to persist for at least a few years. However, it is conceivable that, given an extended interval of low-index AO conditions, ice thickness and summertime sea ice extent could gradually return to the levels characteristic of the 1980's.

Changes in sea ice driven by variations in wind related to the AO appear to be the primary factor forcing the observed decreases in sea ice thickness, and thus the increases in surface air temperature and the decreases in sea ice extent that have been observed since 1989.

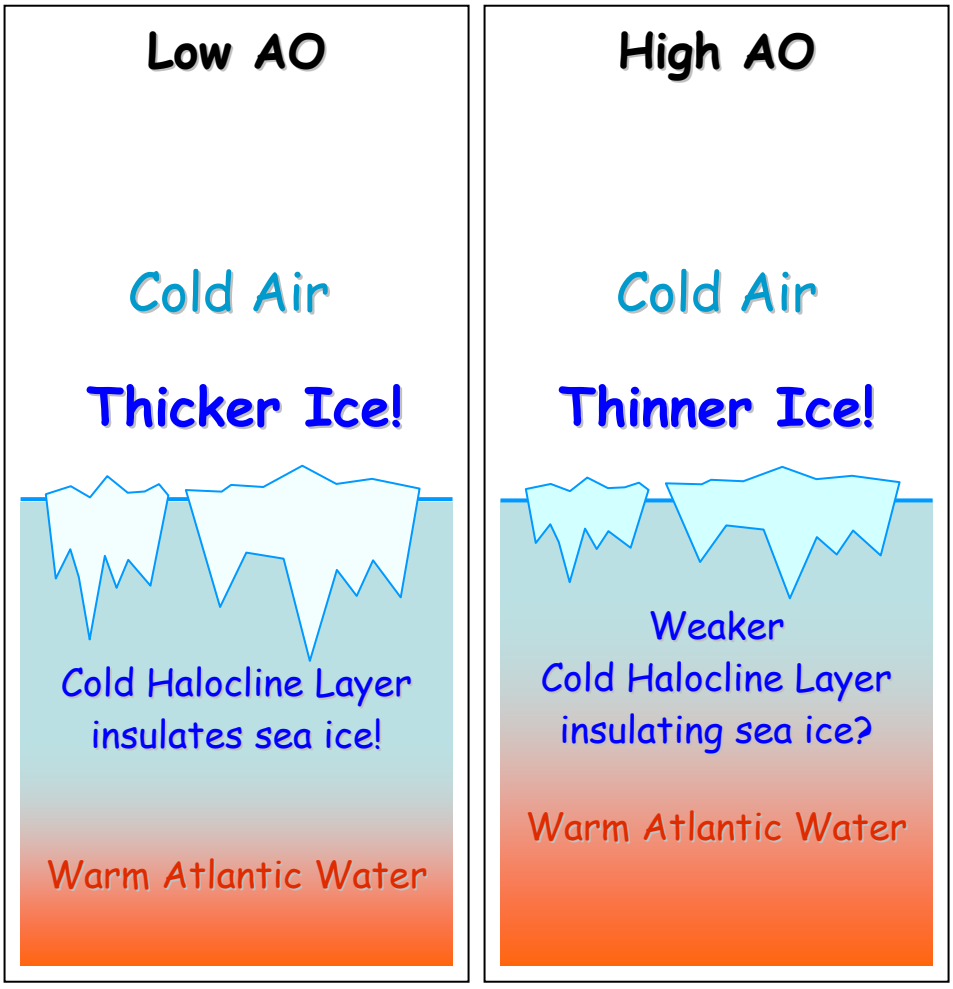

Figure 46. Illustration showing possible changes in the ocean that may affect arctic sea ice during low and high AO conditions.

Here the focus is on the role of changes in wind-driven sea ice motion to explain the recent observed minima in arctic sea ice extent, but it is also possible that changes in the Arctic Ocean during the period of this study may have contributed to the decline. The causal linkages by which changes in the distribution of heat and salt in the ocean could conceivably influence sea ice are shown schematically in Fig. 46. For example, Steele and Boyd (1998) show that the cold halocline layer that insulates the bottom of the sea ice from the warmer Atlantic water below the cold halocline retreated during the 1990's, and Morison et al. (1998) show that the warmer Atlantic water penetrated deeper into the Arctic Ocean during the same period. As summarized by Dickson et al. (2000), results from a number of oceanographic cruises indicate that in comparison with earlier climatologies, the Arctic Ocean in the 1990s was characterized by a more intense and widespread influence of Atlantic-derived waters. These changes in the ocean have also been attributed to a shift in atmospheric circulation over the Arctic in the late 1980's, which coincides with the step to high AO conditions in 1989. Using a global ice-ocean model Zhang et al. (2004) show that the changes in the ocean were strongly correlated with variations in the NAO, and that an increased oceanic flux of heat into the Arctic suppresses the growth of sea ice with a 2–3 year lag. Similarly, Maslowski et al. (2000) conclude that this enhanced inflow of warm, Atlantic-derived waters promotes a stronger upward oceanic heat flux, which may be contributing to the observed decline in arctic sea ice. Subsequent work (Maslowski et al. 2001) suggests an additional role of a warmer inflow of Pacific waters through Bering Strait.

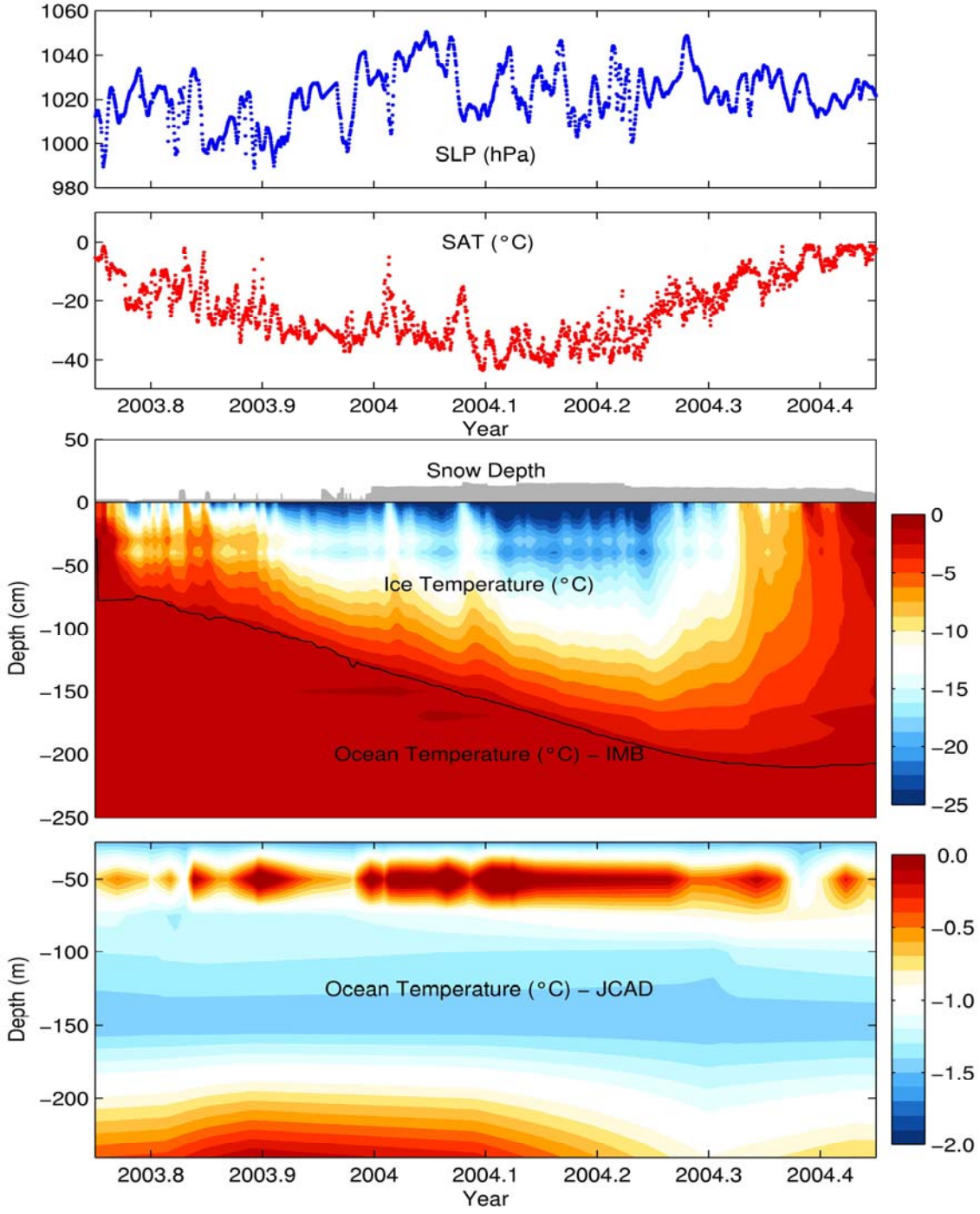

Figure 47. Observations from an International Arctic Buoy Programme Ice Mass Balance (IMB) buoy and JAMSTEC Compact Arctic Drifter (JCAD), which were deployed together on the drifting Arctic sea ice. These buoys measure sea level pressure, surface air temperature, ice thickness and temperatures, snow depth, and ocean temperatures and salinity.

To estimate how much of the observed decline in summer sea ice during the past 15 years is a direct response to changes in the winds and how much of it was an indirect response mediated by the ocean, it will be necessary to perform experiments with coupled climate models that contain improved, realistic sea ice parameterizations. These model parameterizations may be improved by enhancing the observational network over the Arctic Ocean. Towards this end the International Arctic Buoy Programme has recently started deploying buoys that not only measure sea level pressure and surface air temperature, but also sea ice thickness and temperatures, snow depth, and ocean temperatures and salinity. Time series of these data are shown in Fig. 47. From these measurements, a number of other geophysical quantities may be estimated, such as ocean surface heat flux and heat storage. These buoys provide observations of the air, sea ice, and ocean, which can be used for forcing, validation and assimilation into coupled climate models; these may help to improve our understanding of the complex arctic and global climate system.

BIBLIOGRAPHY

Aagaard, K. and E. C. Carmack, The Arctic Ocean and climate: A perspective. The Polar Oceans and Their Role in Shaping the Global Environment: The Nansen Centennial Volume, O.M. Johannessen, R. D. Muench, and J. E. Overland, Eds., Amer. Geophys. Union, pp. 5–20, 1994.

Belkin, I. M., Propagation of the "Great Salinity Anomaly" of the 1990s around the northern North Atlantic, Geophys. Res. Lett., 31, 2004.

Bitz, C. M., 1997: A Model Study of Natural Variability of the Arctic Climate. Ph.D. Dissertation, University of Washington, pp 200.

Bretherton, C.S., C. Smith, and J.M. Wallace, An Intercomparison of Methods for Finding Coupled Patterns in Climate Data, J. Climate, 5, 541–560, 1992.

Comiso, J.C., SSM/I ice concentrations using the Bootstrap algorithm., NASA Report 1380, 1995.

Deser, C., J. E. Walsh, and M. S. Timplin, Arctic sea ice variability in the context of recent atmospheric circulation trends, *J. Climate*, **13**(3), 617–633, 2000.

Dickson, R.R., T.J. Osborn, J.W. Hurrell, The Arctic Ocean response to the North Atlantic Oscillation. *J. Climate* **13**, 2671-2696, 2000.

Drobot S.D., and J.A. Maslanik, Interannual variability in summer Beaufort Sea ice conditions: Relationship to winter and summer surface and atmospheric variability, J. Geophys. Res. Vol. 108(C7), 3233, doi: 10.1029/2002JC001537, 2003.

Fang, Z., Wallace, J.M., Arctic Sea Ice Variability on a Timescale of Weeks and Its Relation to Atmospheric Forcing. *J. Climate*: Vol. 7, No. 12, pp. 1897–1914, 1994.

Haas, C. Dynamics versus Thermodynamics: The Sea Ice Thickness Distribution. Sea Ice, An Introduction to its Physics, Chemistry, Bioloby, and Geology, D. N. Thomas & G. S. Dieckmann Eds., Blackwell, 2003.

Hurrell, J.W., Decadal trends in the North Atlantic Oscillation: Regional temperatures and precipitation. Science, 269, 676-679, 1995.

Jones, P.D., M. New, D.E. Parker, S. Martin, and I.G. Rigor , Surface air temperature and its changes over the past 150 years, *Rev. Geophys.* Vol. 37 , No. 2 , p. 173 - 200, 1999.

Kalnay et al., The NCEP/NCAR Reanalysis Project. Bull. Amer. Meteor. Soc., 77, 437–471, 1996.

Kwok, R., and D. A. Rothrock, Variability of Fram Strait ice flux and North Atlantic oscillation. J. Geophys, Res., 104 (C3), 5177–5189.

Laxon, S., N. Peacock & D. Smith, 2003: High interannual variability of sea ice thickness in the Arctic region, *Nature*, 425 , 947–950.

Lynch, A. H., E. N. Cassano, J. J. Cassano, and L. R. Lestak, Case Studies of High Wind Events in Barrow, Alaska: Climatological Context and Development Processes, Monthly Weather Review: Vol. 131, No. 4, pp. 719–732, 2003.

Makshtas, A.P., S.V. Shoutilin, E.L. Andreas, Possible dynamic and thermal causes for the recent decrease in sea ice in the Arctic Basin. *J. Geophys. Res.* 108 (c7), 2003.

Manabe, S., R. J. Stouffer, M. J. Spelman, and K. Bruan, 1991: Transient response of a coupled ocean-atmosphere model to gradual changes in atmospheric CO_2: Part I. Annual mean response. *J. Climate*, **4**(8), 785–818.

Maslanik, J. A., M. C. Serreze, and T. Agnew, On the record reduction in 1998 western Arctic sea ice cover, *Geophys. Res. Lett*., 26, 1905–1908, 1999.

Maslowski, W., Marble, D.C. & Walczowski, Recent trends in Arctic sea ice. *Ann. Glaciol*., **33**, 545-550, 2001.

Maslowski, W., B. Newton, P. Schlosser, A. Semtner, and D. Martinson, Modeling recent climate variability in the Arctic Ocean. *Geophys. Res. Lett* **27**, 3743-3746, 2000.

Maykut, G. A., Large-scale heat exchange and ice production in the central Arctic. J. Geophys. Res., 87 (C10), 7971–7984.

Morison, J.H., M. Steele, and R. Anderson, Hydrography of the upper Arctic Ocean measured from the nuclear submarine USS Pargo, Deep Sea Res., Part I, 45, 15–38, 1998.

Niebauer, H.J., Variability in Bering Sea ice coveras affected by a regime shift in the North Pacific in the period, 1947–1996, J. Geophys. Res., 103, 27717-27737.

North, G., T. Bell, R. Cahalan, and F. Moeng, Sampling errors in the estimation of empirical orthogonal functions, Mon. Wea. Rev., 110, 699–706, 1982.

Parkinson, C.L., D.L. Cavalieri, P. Gloersen, H.J. Zwally, J. Comiso. Arctic Sea ice extents, areas, and trends, 1978–1996. *J. Geophys. Res., 102 (C6),* 20837–20856, 1999.

Partington, K., T. Flynn, D. Lamb, C. Bertoia, and K. Dedrick, Late twentieth century Northern Hemisphere sea ice record from U.S. National Ice Center ice charts, J. Geophys. Res, 108(C11), doi:10.1029/2002JC001623, 2003.

Pfirman, S.L., R. Colony, D. Nürnberg, H. Eicken, and I. Rigor, Reconstructing the Origin and Trajectory of Drifting Arctic Sea ice, J. Geophys. Res., vol. 102 no.6 pp. 12575-12586, 1997.

Quadrelli, R., and J.M. Wallace, A simplified linear framework for interpreting patterns of Northern Hemisphere wintertime climate variability, J. Climate, accepted, 2004.

Rigor, I.G., R.L. Colony, and S. Martin, Variations in Surface Air Temperature in the Arctic from 1979-1997, *J. Climate*, v. 13, no. 5, pp. 896 - 914, 2000.

Rigor, I.G., J.M. Wallace, R.L. Colony. Response of sea ice to the Arctic Oscillation. *J. Climate, 15, 18*, 2648–2663, 2002.

Rothrock, D.A., Y. Yu, and G.A. Maykut, Thinning of Arctic sea ice. *Geophys. Res. Lett., 26*, 3469–3472, 1999.

Serreze, M.C., J.A. Maslanik, T.A. Scambos, F. Fetterer, J. Stroeve, K. Knowles, C. Fowler, S. Drobot, R.G. Barry, and T.M. Haran. A record minimum arctic sea ice extent and area in 2002. *Geophys. Res. Lett.* 30, 2003.

Shy T.L., and J.M. Walsh. North Pole ice thickness and association with ice motion history. *Geophys. Res. Lett. 23*, 2975–2978, 1996.

Steele, M. and T. Boyd, Retreat of the cold halocline layer in the Arctic Ocean, *J. Geophys. Res.*, 103 (C5), 10,419-10,435, 1998.

Thompson, D. W. J., and J. M. Wallace, The Arctic Oscillation signature in the wintertime geopotential height and temperature fields. *Geophys. Res. Lett.*, **25**(9), 1297–1300, 1998.

Thorndike, A. S., and R. Colony, 1982: Sea ice motion in response to geostrophic winds. *J. Geophys. Res*., **87**(C8), 5845–5852.

Thorndike, A.S.: Kinematics of Sea Ice. NATO advanced science institutes series. Series B, Physics, The geophysics of sea ice / Edited by N. Untersteiner. v.146, 1989, p.489–550.

Wallace, J. M., and D. S. Gutzler, 1981: Teleconnections in the geopotential height field during the Northern Hemisphere Winter. *Mon. Wea. Rev.*, **109,** 784-812.

Wallace, John M., Smith, Catherine, Bretherton, Christopher S. 1992: Singular Value Decomposition of Wintertime Sea Surface Temperature and 500-mb Height Anomalies. *Journal of Climate*: Vol. 5, No. 6, pp. 561–576.

Walsh, J. E., and M. Timlin, 2003: Northern Hemisphere sea ice simulations by global climate models, *Polar Research*, 22(1), 75 -82.

Walsh, J. E; Chapman, W. L; Shy, T. L., Recent decrease of sea level pressure in the central Arctic, Journal of Climate, Boston, MA. Vol. 9, no. 2, pp. 480-486. 1996.

Walsh, J. E., and H. J. Zwally, 1990: Multiyear sea ice in the Arctic: model- and satellite-derived. *J. Geophys. Res*., 95, 11613–11628.

Walsh, J.E. A data set on Northern Hemisphere sea ice extent. World Data Center-A for Glaciology (Snow and Ice), "Glaciological Data, Report GD-2", part 1, pp. 49–51, 1978.

Wongittilin Sr., J. Alaska Traditional Knowledge and Native Foods Database, Alaska Native Science Commission and Institute of Social and Economic Research, http://www.nativeknowledge.org/, 2000.

Yu, Y. D.A. Rothrock, and G.A. Maykut. Changes in Thickness Distribution of Arctic Sea ice between 1958–1970 and 1993–1997. *J. Geophys. Res.*, in press.

Zhang, J., M. Steele, D. Andrew Rothrock, and R. W. Lindsay, Increasing exchanges at Greenland-Scotland Ridge and their links with the North Atlantic Oscillation and Arctic Sea Ice, *Geophys. Res. Lett.*, v. 31, 2004.

Zhang, J., and D.A. Rothrock, 2003: Modeling global sea ice with a thickness and enthalpy distribution model in generalized curvilinear coordinates, *Mon. Wea. Rev*., 131(5), 681-697.

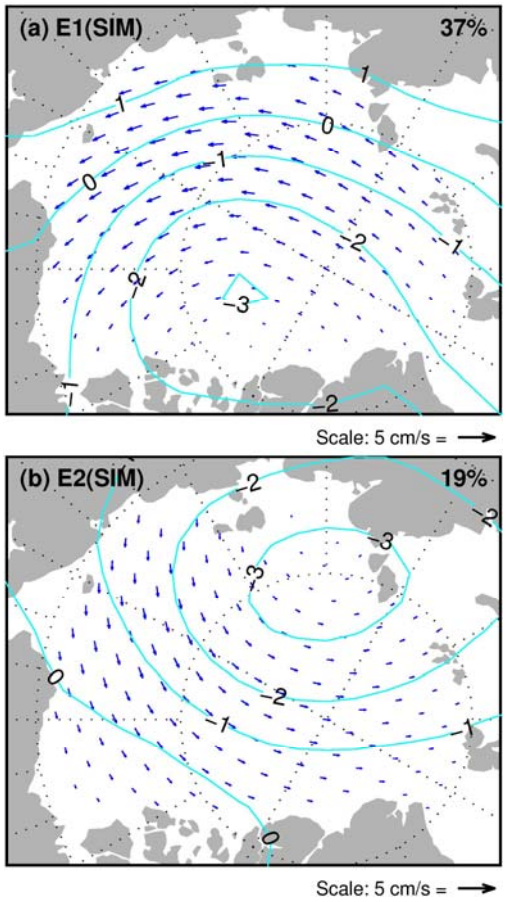

Figure 48. Regression maps of sea ice motion and sea level pressure on the first two EOF PCs of sea ice motion for 1955–1978.

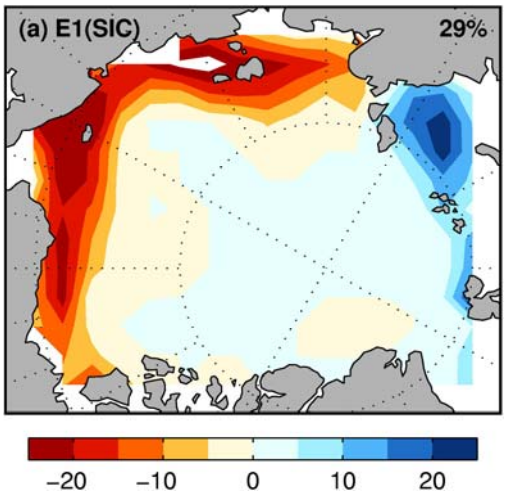

Figure 49. Regression maps of sea ice concentration on the first EOF PC of September sea ice concentration for 1955–1978.

Appendix A: EOFs of Sea ice Motion and Sea ice Concentration for 1955-1978.

The number of observations available for the optimal interpolation of sea ice motion fields prior to 1979 were limited (Fig. 15). However, given the long correlation length scale between the observations of monthly sea ice motion (Pfirman et al. 1997) we were still able to estimate sea ice motion fields from 1955 to 1978. The quality of the sea ice motion data can be inferred from the correspondence between these sea ice motion fields and the sea level pressure fields prior to 1979 (Fig. 48). The EOF of sea ice motion for this shorter period reproduces the primary modes of variability of sea ice motion found for the full period of this study (Fig. 21), and the sea ice motion fields are highly correlated with the sea level pressure fields.

The sea ice concentration data exhibit a discontinuity related to the introduction of passive microwave satellite data to estimate sea ice concentration (Deser et al. 2000). Beginning in 1978 estimates of sea ice concentration are lower, especially over the perennial ice pack. Figure 49 shows the regression of sea ice concentration on the first PC from the EOF analysis of sea ice concentration from 1955 to 1978. This analysis reproduces the same patterns of variability found over the full 48-year period (Fig. 18).

VITA

Ignatius G. Rigor was born in Agana, Guam on October 24, 1964, to Maria Paz Ganzon, and Thomas V. Rigor Jr. He grew up as a "Navy Brat," traveling between the U.S. and the Philippines before he moved to Seattle in December 1978.

He graduated from Blanchet High School in 1981 and received a Bachelor of Science in Cell nd Molecular Biology from the University of Washington in 1986. Through college he worked at the Polar Science Center, Applied Physics Laboratory of the University of Washington, and was offered a job as a Mathematician upon graduating.

In 1998 he began graduate studies in the Department of Atmospheric Sciences at the University of Washington. In 2001 he finished his Masters of Science in Atmospheric Sciences, and in 2004 he finished his Doctor in Philosophy in Atmospheric Sciences.